International Journal of Heat and Fluid Flow 73 (2018) 236–257

Interface methods for grey-area mitigation in turbulence-resolving hybrid RANS-LES

S. Arvidson[1,2], L. Davidson[2] and S-H. Peng[2,3]

[1]Saab Aeronautics, SE-581 88 Linköping, Sweden,
sebastian.arvidson@saabgroup.com

[2]Division of Fluid Dynamics, Department of Mechanics and Maritime Sciences,
Chalmers University of Technology,
SE-412 96 Gothenburg, Sweden

[3]Swedish Defence Research Agency (FOI), SE-164 90 Stockholm, Sweden

Keywords: Hybrid RANS-LES turbulence modeling, RANS-LES interface, embedded LES, grey-area mitigation, commutation terms

Abstract

A grey area mitigation method is proposed for hybrid RANS-LES. The proposed methodology is evaluated using a hybrid RANS-LES method based on a Low-Reynolds-Number $k-\omega$ model applied to channel flow, boundary layer flow and a spatially developing mixing layer flow. Emphasis is put on the use of commutation terms at the RANS-LES interfaces in the transport equations for the turbulent kinetic energy, the specific dissipation rate and the momentum equation in order to rapidly reduce the turbulent viscosity across a RANS-to-LES interface and to stimulate the development of resolved turbulent fluctuations. The proposed methodologies are applied at both wall-normal (and inlet) and wall-parallel RANS-LES interfaces.

The proposed methodology gives a rapid reduction of the turbulent viscosity at the wall-normal RANS-LES interface from its RANS level to its LES level. Moreover, the proposed methodology contributes to a substantially more rapid establishment of the turbulence-resolving LES flow downstream of the wall-normal RANS-LES interface than if no grey-area mitigation method is applied. However, the proposed methodology has a weaker effect at wall-parallel RANS-LES interfaces, due to a stronger entrainment of LES contents into the near-wall RANS region, than at the wall-normal RANS-LES interfaces.

Good agreement with experimental data is obtained with the proposed interface method for the evaluated flow cases. The most obvious grey area mitigation effect is given in the simulated mixing layer flow. Turbulent velocity fluctuations are efficiently established with the commutation term in the momentum equation at the RANS-LES interface in this flow as well as a rapid reduction of the turbulent viscosity due to the commutation terms in the k and ω equations, which gives an almost negligible delay in the development of the resolved turbulence.

1 Introduction

The requirement for increased accuracy in simulations of industrial flows drives the needs for robust and cost-effective turbulence-resolving methods. It is well known that Large-Eddy Simulation (LES) is associated with a very high computational cost when applied to high-Reynolds-number flows and that the use of LES in e.g. aeronautical flows will not be possible in the next decades [1]. Reynolds-Averaged Navier-Stokes (RANS) on the other hand is computationally much less costly than LES but suffers from inaccuracy when applied to separated flows. However, a combination of RANS and LES (hybrid RANS-LES) gives the accuracy needed in separated flows and an affordable computational cost for attached high-Reynolds-number flows.

Still, for hybrid RANS-LES methods the computational cost is orders of magnitudes larger than for RANS simulations. There is thus a strong need for embedded approaches where turbulence-resolving methods can be used in specific flow regions with e.g. separated flow and RANS can be used elsewhere. Examples of such turbulence-resolving methods can be, Detached-Eddy Simulation (DES) type methods [2, 3, 4] or zonal RANS-LES methods [5, 6, 7]. This paper focuses on zonal RANS-LES methods.

In combined RANS and LES simulations, the absence of resolved turbulence in the RANS simulated flow gives rise to a transition region in the LES simulated flow, where the resolved turbulent stresses are not fully developed. This transition

region, called the grey area, was first highlighted by Spalart et al. [2]. Since then, great research efforts has been put into mitigating this grey area phenomenon, e.g. in the EU-FP7 Go4Hybrid project [8].

Accurate predictions of free shear layers, using hybrid RANS-LES methods, require a rapid development of the resolved turbulent stresses when the model in switched from RANS to LES. To accelerate the transition from RANS to LES and thus mitigate the grey area, Kok and van der Ven [9] proposed a stochastic subgrid scale model and a high-pass filtered subgrid scale model.

Different LES length scales have been proposed in which the filter width is adapted to the local flow situation. For example, Chauvet et al. [10] proposed a LES length scale based on the local vorticity field in order to minimize the excess of subgrid scale (SGS) turbulent viscosity in free shear layer flows. This length scale was further developed by Mockett et al. [11] and Shur et al. [12] and has been evaluated in different DES-type models. Mockett et al. [11] also proposed the use of alternative SGS models that better adapt to the local flow field compared to the commonly used Smagorinsky model with the aim to further reduce the RANS-to-LES transition region in e.g. free shear layer flows.

In attached boundary layer flows and mildly separated flows, where no strong natural instabilities are present, an addition of synthetic turbulent fluctuations at the RANS-LES interface can be needed, due to the absence of resolved turbulence in the oncoming RANS simulated flow, to force a rapid development of the turbulence-resolving LES flow. By superimposing synthetic turbulent fluctuations onto the RANS mean flow field at the RANS-to-LES interface, additional turbulent energy is introduced. Hence, a transfer of modeled turbulent kinetic energy to resolved turbulent kinetic energy (i.e. a reduction of the modeled turbulent kinetic energy) must be made to avoid an excess of turbulent kinetic energy on the LES side of the interface. In e.g. Arvidson et al. [13], the reduction of modeled turbulent kinetic energy from its RANS level to its estimated SGS level was prescribed using an empirical constant.

Hamba [14] used filtered DNS data to explore the commutation error, owing to the non-commutivity of the spatial derivative and the filter applied in RANS and LES, at the RANS-LES interface. He argued that the commutation error can be large across the RANS-LES interface and thus needs to be considered. Girimaji and Wallin [15] applied Hamba's theory to Partially-Averaged Navier-Stokes (PANS) simulations of Decaying Homogeneous Isotropic Turbulence (DHIT). They showed that the proposed commutation terms can be used to give the required transfer of modeled-to-resolved/resolved-to-modeled turbulent kinetic energy without any use of empirical constants. The commutation terms proposed by Hamba were further explored by Davidson [16, 17] and Arvidson [7] in combination with synthetic turbulent fluctuations at interfaces in hybrid RANS-LES simulations with the aim to reduce the RANS turbulent viscosity to SGS levels and to promote a rapid growth of the turbulence-resolving LES flow.

In this paper, we explore the effect of commutation terms in turbulence-resolving simulations using a low-Reynolds-number $k-\omega$ based hybrid RANS-LES turbulence model [7]. We apply the proposed methodology to embedded LES simulations of channel flow, boundary layer flow and mixing layer flow.

The paper is organized as follows. First, a short description of the numerical procedure is given, which is followed by a description of the turbulence model used. There is then a presentation of the proposed commutation terms and the method used for generating the synthetic turbulent fluctuations applied at the RANS-LES interfaces. The results are presented in the section that follows, and the effect of the commutation terms are evaluated. The final section gives the conclusions that are drawn from the methods applied.

2 Modeling and simulation methods

2.1 Numerical procedure

An incompressible solver based on a finite volume technique was used in this paper. The temporal advancement is made with the second order Crank-Nicolson scheme. A first order upwind/hybrid scheme is used as spatial discretization for the turbulent transport equations. The spatial discretization of the momentum equations is presented for each test case. An implicit, fractional step technique with a multigrid Poisson solver was used on a non-staggered grid arrangement. For a more detailed description of the numerical procedure, see Davidson and Peng [5].

2.2 Zonal hybrid RANS-LES model

The formulation of the zonal hybrid RANS-LES model [7], based on the PDH-LRN $k-\omega$ model [18], is presented below.

$$\frac{D\rho k}{Dt} = \tau_{ij}\frac{\partial u_i}{\partial x_j} - D^k + \frac{\partial}{\partial x_j}\left[\left(\mu + \frac{\mu_t}{\sigma_k}\right)\frac{\partial k}{\partial x_j}\right] \tag{1}$$

$$D^k = C_k f_k \rho k\omega = \rho f_k \frac{k^{3/2}}{l_t} \tag{2}$$

$$\frac{D\rho\omega}{Dt} = C_{\omega_1} f_\omega \frac{\omega}{k} \tau_{ij} \frac{\partial u_i}{\partial x_j} - C_{\omega 2} \rho \omega^2 + \frac{\partial}{\partial x_j}\left[\left(\mu + \frac{\mu_t}{\sigma_\omega}\right)\frac{\partial \omega}{\partial x_j}\right] + C_\omega \frac{\mu_t}{k}\frac{\partial k}{\partial x_j}\frac{\partial \omega}{\partial x_j} \tag{3}$$

$$\mu_t = C_\mu f_\mu \frac{\rho k}{\omega} \tag{4}$$

$$f_k = 1 - 0.722 \cdot \exp\left[-\left(\frac{R_t}{10}\right)^4\right] \tag{5}$$

$$f_\omega = 1 + 4.3 \cdot \exp\left[-\left(\frac{R_t}{1.5}\right)^{1/2}\right] \tag{6}$$

$$f_\mu = 0.025 + \left\{1 - \exp\left[-\left(\frac{R_t}{10}\right)^{3/4}\right]\right\}\left\{0.975 + \frac{0.001}{R_t}\exp\left[-\left(\frac{R_t}{200}\right)^2\right]\right\} \tag{7}$$

On the left hand side of the transport equations, D/Dt is the material derivative, $D/Dt = \partial/\partial t + u_i \partial/\partial x_i$. The variables u_i, k, ω and μ_t in the transport equations are, respectively, the velocity components, turbulent kinetic energy, specific dissipation rate of k and the turbulent viscosity. To achieve a correct near-wall modeling, the low-Reynolds-number damping functions f_k, f_ω and f_μ are used, where $R_t = k/(\nu\omega)$ is the turbulent Reynolds number. The model constants are: $\sigma_k = 0.8$, $\sigma_w = 1.35$, $C_\mu = 1.0$, $C_k = 0.09$, $C_{\omega 1} = 0.42$, $C_{\omega 2} = 0.075$ and $C_\omega = 0.75$. In the present paper, the modeling modes, i.e. RANS or LES, are prescribed such that the switch occurs at a specific grid line and the turbulent length scale, l_t, is adapted to the modeling mode so that $l_t = l_{RANS} = k^{1/2}/(C_k\omega)$ in RANS mode and $l_t = l_{LES} = \Psi_{PDH} C_{LES} \Delta$ in LES mode. In LES mode Δ, represented by the three different formulations in Eqs. (8-10), is the LES filter width, and $C_{LES} = 0.70$, and $\Psi_{PDH} = \min\left[10, f_k\left(f_\omega/f_\mu\right)^{3/4}\right]$ is the correction function used to avoid the low-Reynolds-number damping effect in the LES region. For details about C_{LES} and the correction function, see Arvidson et al. [13]. The wall boundary condition for ω is set to $\omega = 6\nu/\left(C_{\omega 2} y^2\right)$ at the wall-adjacent cells.

$$\Delta_{dw} = \min\left(\max\left[C_{dw} d_w, C_{dw}\Delta_{max}, \Delta_{nstep}\right], \Delta_{max}\right) \tag{8}$$

$$\Delta_{max} = \max\left(\Delta_\xi, \Delta_\eta, \Delta_\zeta\right) \tag{9}$$

$$\begin{aligned} \Delta_\Omega &= \sqrt{N_\xi^2 \Delta_\eta \Delta_\zeta + N_\eta^2 \Delta_\xi \Delta_\zeta + N_\zeta^2 \Delta_\xi \Delta_\eta} \\ \boldsymbol{N} &= \frac{\boldsymbol{\Omega}}{\parallel \boldsymbol{\Omega} \parallel}, \qquad \boldsymbol{\Omega} = \nabla \times \boldsymbol{u} \end{aligned} \tag{10}$$

In the length scale, Δ_{dw} (Eq. (8)), which was proposed by Shur et al. [4] and used in Improved Delayed Detached-Eddy Simulation (IDDES), d_w is the wall distance and $C_{dw} = 0.15$. Δ_{nstep} is the grid cell size in the wall-normal direction. The LES length scale Δ_{max} represents the maximum edge length of the local control volume. The LES length scale Δ_Ω, proposed by Jauvet et. al [10], adapts to the local vorticity field in order to minimize the excess of SGS turbulent viscosity. In the equations, Δ_ξ, Δ_η, and Δ_ζ are the sizes in the ξ, η and ζ directions, respectively, of the local control volume in a curvilinear grid with hexahedral cells. In Eq. (10), $\boldsymbol{N}$ is the direction of the spin axis of the local vorticity.

2.3 Commutation error at the RANS-LES interfaces

A commutation error occurs in hybrid RANS-LES simulations since the hybrid filter does not commute with the spatial derivative. Due to this non-commutivity, an additional term appears when computing the spatial derivative of a physical quantity f, as shown in Eq. (11).

$$\frac{\overline{\partial f}}{\partial x_i} = \frac{\partial \overline{f}}{\partial x_i} - \frac{\partial \Delta}{\partial x_i}\frac{\partial \overline{f}}{\partial \Delta} \tag{11}$$

The analysis below is made in order to show how Eq. (11) can be reached. The analaysis is made in one dimension for simplicity. The physical variable $\overline{f}(x)$ is defined as in Hamba [14]

$$\overline{f}(x) = \int_{-\infty}^{\infty} G\left(x - x', \Delta(x)\right) f\left(x'\right) dx' \tag{12}$$

where G is the filter function and Δ is the filter width, which represents a length scale range from LES to RANS depending on which modeling mode that is used as in Hamba [14]. Make the substitution $s = x - x'$ which gives $ds = -dx'$ and insert into Eq. (12).

$$\begin{aligned} \overline{f}(x) &= \int_{\infty}^{-\infty} G\left(s, \Delta(x)\right) f\left(x - s\right) (-ds) \\ &= \int_{-\infty}^{\infty} G\left(s, \Delta(x)\right) f\left(x - s\right) ds \end{aligned} \tag{13}$$

Compute the derivatie with respect to x

$$\begin{aligned} \frac{\partial \overline{f}}{\partial x} &= \frac{\partial \overline{f}}{\partial \Delta}\frac{d\Delta}{dx} + \int_{-\infty}^{\infty} G\left(s, \Delta(x)\right) \frac{\partial f}{\partial x}\left(x - s\right) ds \\ &= \frac{\partial \overline{f}}{\partial \Delta}\frac{d\Delta}{dx} + \overline{\frac{\partial f}{\partial x}} \end{aligned} \tag{14}$$

Finally, Eq. (11) is given by re-arranging the terms in Eq. (14).

Since it has been shown that the commutation error can be large at the RANS-LES interfaces [14], we explore in this paper the effects of commutation terms in the hybrid RANS-LES turbulence model formulation, described above, in simulations of embedded LES of channel flow, boundary layer flow and spatially developing mixing layer flow. We chose in the present paper to introduce the commutation terms for the convection terms in the k, ω and momentum equations. Even though the grid used in this work are streched, a smooth grid streching is applied which gives that that the term $\partial\Delta/\partial x_i$ in Eq. (11) is small. Therefore, the commutation error due to the non-homogeneous grid in the LES region is omitted since this effect is much smaller than the effect of switching the modeling mode at the RANS-LES interfaces.

Using Eq. (11), the commutation term for the convection in the modeled k equation can be formulated as

$$\overline{\frac{\partial u_i k}{\partial x_i}} = \frac{\partial \overline{u}_i k}{\partial x_i} - \underbrace{\frac{\partial \Delta}{\partial x_i}\frac{\partial \overline{u}_i k}{\partial \Delta}}_{S_k^c} \tag{15}$$

A corresponding term can be formulated for the convection term in the ω equation. The ω equation is derived by transforming the k and ϵ equations. It is assumed that the dissipation rate (ϵ) is not affected across the RANS-LES interface. This means that the viscous dissipation rate dominates over the dissipation rate due to the resolved turbulence. Since the simulations presented are performed on grids much coarser than DNS resolution grids, which are required in order to achieve an accurate dissipation rate because of the resolved turbulence, the assumption is valid. To derive the commutation term in the ω equation, start from the ϵ equation and multiply by $1/\left(C_k k\right)$

$$\frac{d\omega}{dt} = \frac{d}{dt}\left(\frac{\epsilon}{C_k k}\right) = \frac{1}{C_k k}\frac{d\epsilon}{dt} + \frac{\epsilon}{C_k}\frac{d(1/k)}{dt} = \frac{1}{C_k k}\frac{d\epsilon}{dt} - \frac{\omega}{k}\frac{dk}{dt} \tag{16}$$

From Eq. (16) it can be seen that the source terms in the ω equation are given by the source terms in the ϵ equation multiplied by $1/\left(C_k k\right)$ and the source terms in the k equation multiplied by $-\omega/k$. This leads to the following commutation term in the ω equation

$$\overline{\frac{\partial u_i \omega}{\partial x_i}} = \frac{\partial \overline{u}_i \omega}{\partial x_i} - \frac{\partial \Delta}{\partial x_i}\frac{\partial \overline{u}_i \omega}{\partial \Delta} = \frac{\partial \overline{u}_i \omega}{\partial x_i} + \frac{\omega}{k}\frac{\partial \Delta}{\partial x_i}\frac{\partial \overline{u}_i k}{\partial \Delta} = \frac{\partial \overline{u}_i \omega}{\partial x_i} + \underbrace{\frac{\omega}{k} S_k^c}_{S_\omega^c} \tag{17}$$

By adding the commutation terms in the k and ω equations at the RANS-LES interface, the aim is to reduce the grey area in LES. The source term added to the k equation acts to reduce the modeled turbulent kinetic energy for a flow directed across the interface from RANS to LES. Since the source term in the ω equation has the opposite sign to that

of the source term in the k equation, the commutation term increases the specific dissipation rate. Hence, for a flow across the interface with the direction from RANS to LES, a reduction of the turbulent viscosity will be obtained with a possibility to mitigate the grey area.

The commutation term introduced in the k equation contributes to a change in the modeled turbulent kinetic energy across the RANS-LES interface. This change should be compensated with a change of the resolved turbulent kinetic energy. For example, when the modeled turbulent kinetic energy is reduced across a RANS-to-LES interface due to S_k^c, the resolved turbulent kinetic energy should be increased by the same amount across the interface. This energy transfer is achieved by introducing a source term in the momentum equations, which should represent a commutation term in the transport equation for resolved turbulent kinetic energy.

The transport equation for resolved turbulent kinetic energy is derived by subtracting the time-averaged momentum equations from the instantaneous momentum equations to get the momentum equations for a fluctuating velocity. Each term in this equation are multiplied by $\overline{u}_i'$ and time-averaged. The source term introduced in the momentum equations is in this paper based on the source term S_k^c, representing the commutation error for the convection term in the k equation. The time-average of the source term in the momentum equations for the fluctuating velocity multiplied by the velocity fluctuation should thus be found in the transport equation for resolved turbulent kinetic energy, i.e. $\langle S_k^c \rangle$. The source term introduced in the momentum equations can take the form

$$S_i^1 = \langle S_k^c \rangle \frac{\overline{u}_i'}{\langle \overline{u}_m' \overline{u}_m' \rangle} \tag{18}$$

Now multiply Eq. (18) by $\overline{u}_i'$ and time average

$$\left\langle \langle S_k^c \rangle \frac{\overline{u}_i'}{\langle \overline{u}_m' \overline{u}_m' \rangle} \overline{u}_i' \right\rangle = \langle S_k^c \rangle \frac{\langle \overline{u}_i' \overline{u}_i' \rangle}{\langle \overline{u}_m' \overline{u}_m' \rangle} = \langle S_k^c \rangle \tag{19}$$

As seen, Eq. (19) is equal to the time-average of Eq. (15), but with opposite sign, as it should.

To ensure that S_i^1 has the same sign as the velocity fluctuation itself in order to act as a modeled turbulence generator at the RANS-LES interface and thus enforce the velocity fluctuations, the `sign` function is introduced. Finally, the used source term in the momentum equations reads

$$S_{mom,i}^c = \texttt{sign}\left(u_i'\right) \left| \langle S_k^c \rangle \frac{u_i'}{\langle u_m' u_m' \rangle} \right|. \tag{20}$$

A similar term was proposed by Davidson [16] and used in zonal PANS simulations of channel flow.

It should be noted that the introduction of $S_{mom,i}^c$ requires a running time-average. In the simulations presented in this paper, typically 1000 time-steps were required to establish the time-averaged velocities from a fully developed flow. Another 1000 time steps were needed to establish the effect of the commutation terms in the momentum equations.

The source terms introduced in the momentum equations (Eq. (20)) are added only on the LES side of the interface, i.e. it is added only when the local flow direction is from RANS to LES across the RANS-LES interface. $S_{mom,i}^c$ is ensured to have the same sign as the velocity fluctuation on the LES side of the interface to enforce the turbulent fluctuations (i.e. increase the resolved turbulent kinetic energy) at the same time as the modeled turbulent kinetic energy (and the turbulent viscosity) are reduced by the source term introduced in the k (and ω) equation on the LES side of the interface.

It is important to note that the proposed methodology does not involve any empirical constants or functions. Moreover, it is a general method that can be applied to any transport equation based hybrid RANS-LES turbulence model. To discretize the source term S_k^c around the RANS-LES interface, a finite difference approximation is applied as in Hamba [14], see the sections below.

2.3.1 Wall-normal interface

In the simulations in which the RANS-LES interface is aligned with the inlet, i.e. a wall-normal interface, four combinations for how the source terms, representing the commutation error and synthetic turbulent fluctuations (STF), have been applied are shown in Fig. 1.

In strategy 1, commutation terms are added in the k and ω equations in order to rapidly reduce the turbulent viscosity on the LES side of the RANS-LES interface.

Using strategy 2, commutation terms are added in the k, ω and momentum equations. The source term in the momentum equations acts as a modeled turbulence generator in order to further promote the growth of the resolved turbulence.

With strategy 3, STF (see Section 2.4) are added as source terms in the momentum equations ($S_{i,mom}^s$) at the wall-normal RANS-LES interface (or inlet plane) without any commutation terms.

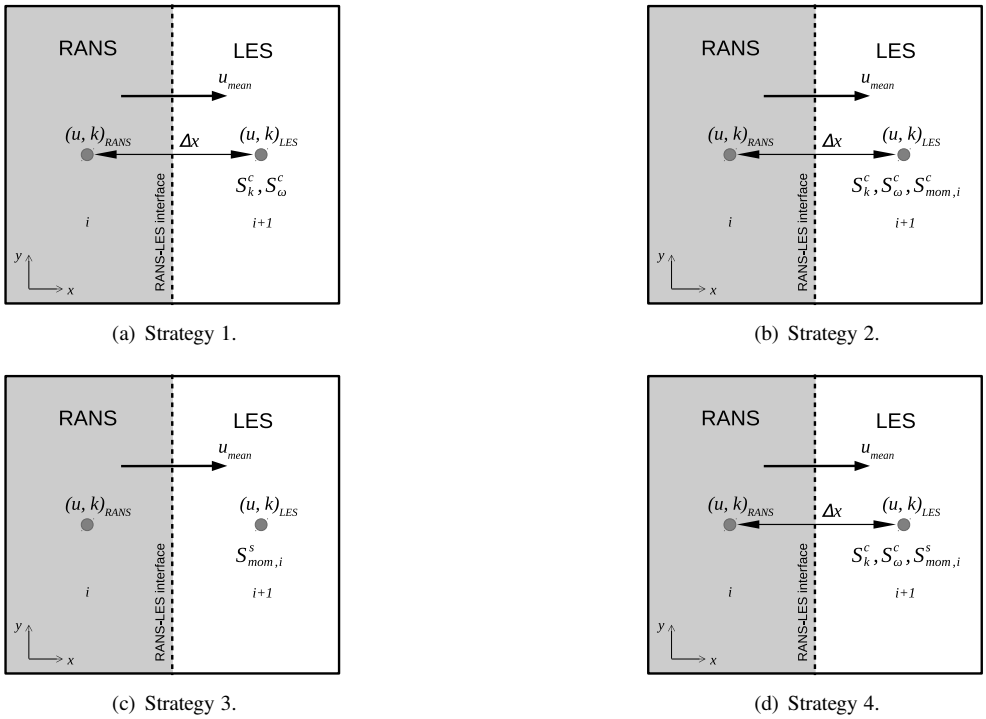

(a) Strategy 1.

(b) Strategy 2.

(c) Strategy 3.

(d) Strategy 4.

Figure 1: Strategies for the wall-normal RANS-LES interface. RANS and LES cells, adjacent to the RANS-LES interface are shown, with source terms for commutation error (S_k^c, S_ω^c and $S_{mom,i}^c$) and synthetic turbulent fluctuations ($S_{mom,i}^s$).

Strategy 4 uses the commutation terms in the k and ω equations to reduce the turbulent viscosity on the LES side of the interface, and STF are added to the momentum equations as source terms in order to speed up the formation of the turbulence resolving flow.

Table 1 shows applications to which the different interface strategies have been applied. The strategies used for the wall-parallel RANS-LES interfaces are also included but are described in Section 2.3.2.

Table 1: Methodologies applied to the RANS-LES interfaces for different flow cases. A zero indicates that no commutation terms and no STF are added at the RANS-LES interfaces.

Flow case	Strategy for wall-normal interface or inlet plane	Strategy for wall-parallel interfaces
Channel flow	3, 4	0, 1, 2, 3
Boundary Layer	3, 4	0, 1, 2, 3
Mixing layer	0, 1, 2	N/A

For a wall-normal interface, the following discretization of S_k^c is used

$$\begin{aligned} S_k^c &= \frac{\partial \Delta}{\partial x}\frac{\partial \overline{u}k}{\partial \Delta} = \left(\frac{\Delta_{LES}-\Delta_{RANS}}{\Delta x}\right)\frac{\overline{u}_{RANS}k\left(x\right)-\overline{u}_{LES}k_{LES}}{\Delta_{RANS}-\Delta_{LES}} \\ &= \frac{\overline{u}_{LES}k_{LES}-\overline{u}_{RANS}k\left(x\right)}{\Delta x} \end{aligned} \tag{21}$$

where Δx is the distance between the cell centers at the RANS and LES locations, here indicated by the subscripts $RANS$ and LES, respectively, on each side of the interface, as shown in Fig. 1.

The value of k_{LES} is the estimated SGS turbulent kinetic energy computed according to Eq. (22). The value of $k\left(x\right)$ (without any subscript in Eq. (21)) is set to the value at the current cell i, i.e. it represents the solution of Eq. (1), and not its RANS value. This is done in order to achieve a smoother reduction of k across a RANS-to-LES interface and to avoid stability problems.

$$k_{LES} = \left(\frac{\nu_{sgs}}{\Delta}\right)^2, \nu_{sgs} = (C_s\Delta)^2 \left|\overline{s}\right|, C_s = 0.1 \tag{22}$$

The filter width used to estimate k_{LES} in Eq. (22) corresponds to the filter width used for the LES length scale in the dissipation term in the transport equation for the turbulent kinetic energy (Eq. (1)). It should be noted that there is no explicit dependency of Δ in Eq. (21)) since it is assumed that Δ and k varies linearly between the RANS and the LES locations. Hence, the RANS and LES length scales in the nominator and the denominator cancel each other. However, Δ is implicitly involved in S_k^c since it is assumed that k varies between k_{RANS} and k_{LES}.

The influence of the distance x_{tr}, which is the length of the region in which the commutation terms are used in the k and ω equations, has been analyzed by Davidson [19], where he concluded that the larger the x_{tr}, the weaker the effect of the commutation terms. In this work, $x_{tr} = \Delta x$ is the distance between the adjacent cell centers at each side of the RANS-LES interface. Even though the proposed commutation term gives a strong impact on the production of the modeled turbulent kinetic energy with such a small distance between the RANS and LES locations, this distance between the adjacent cells is well-defined also when considering complex grids.

It has been shown by e.g. Davidson [20] that the turbulent viscosity level in the near-wall RANS region in hybrid RANS-LES simulations is much lower than the turbulent viscosity in the near-wall region in RANS simulations of the same flow. The commutation terms are thus also added in the near-wall RANS region to rapidly adapt the RANS simulated near wall flow to a lower turbulent viscosity level. This means that the methodology is applied across the entire embedded RANS-LES interface (or inlet boundary).

2.3.2 Wall-parallel interface

Three strategies for applying the commutation terms in the k, ω and the momentum equations at the wall-parallel RANS-LES interface have been evaluated, as shown in Fig. 2, where v_{int} is the instantaneous velocity orthogonal to the RANS-LES interface and is used as a sensor to determine if the flow direction is from RANS to LES or vice-versa across the interface. The velocity v_{int} is evaluated at the cell face between cell j and $j+1$.

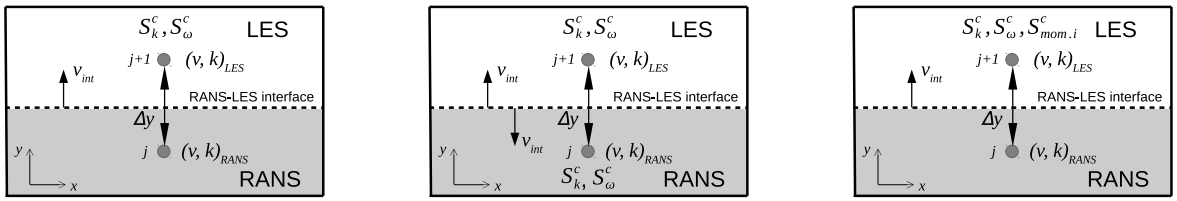

(a) Strategy 1. (b) Strategy 2. (c) Strategy 3.

Figure 2: Strategies for the wall-parallel RANS-LES interface. RANS and LES cells, adjacent to the RANS-LES interface, with source terms for commutation errors (S_k^c, S_ω^c and $S_{mom.i}^c$).

In the first strategy shown in Fig. 2 (a), the commutation terms in the k and ω equations have been applied only on the LES side of the interface when the flow direction across the interface, i.e. v_{int}, is from RANS to LES. When the flow direction is from the LES region to the RANS region, the commutation terms are set to zero.

In the second strategy, as shown in Fig. 2 (b), the commutation terms in the k and ω equations have been added on both sides of the interface. When the direction of the flow across the interface is from the RANS region to the LES region, the commutation terms on the LES side of the interface reduce the turbulent viscosity in the LES region. When the flow direction across the interface is from LES to RANS, the commutation terms are added on the RANS side on the interface in order to increase the turbulent viscosity in the RANS region.

The third strategy shown in Fig. 2 (c) is similar to strategy 1, but in addition to the comutation terms in the k and ω equations the source term $S_{mom,i}^c$ in the momentum equations is added on the LES side of the interface when the flow direction across the interface is from RANS to LES. Table 1 in the previous section summarizes to which flow cases the different interface strategies have been applied.

The discretized form of S_k^c, used at the wall-parallel RANS-LES interface, reads

$$\begin{aligned} S_k^c &= \frac{\partial\Delta}{\partial y}\frac{\partial\overline{v}k}{\partial\Delta} = \left(\frac{\Delta_{LES}-\Delta_{RANS}}{\Delta y}\right)\frac{\overline{v}_{RANS}k\left(y\right)-\overline{v}_{LES}k_{LES}}{\Delta_{RANS}-\Delta_{LES}} \\ &= \frac{\overline{v}_{LES}k_{LES}-\overline{v}_{RANS}k\left(y\right)}{\Delta y} \end{aligned} \tag{23}$$

As in Eq. (21), k_{LES} is computed according to Eq. (22) and $k\,(y)$ without any subscript is taken at cell j. Moreover, Δy is the distance between the cell centers adjacent to the RANS-LES interface. Note that it is assumed in Eq. (23) that the velocity v is positive across a RANS-to-LES interface. Thus, at the upper wall in the channel flow, the sign of S_k^c has to be taken care of so that this term acts as a sink term in the k equation for a flow going from RANS to LES.

Due to the formulation of the RANS flux $(v_{RANS}k(y))$ for the turbulent kinetic energy in Eq. (23) and the fact that the modeled turbulent kinetic energy is larger on the RANS side of the interface than on the LES side, the contribution from the commutation terms will be stronger on the RANS side of the interface than on the LES side.

It was observed that, instantaneously, the magnitude of the commutation term in the momentum equations, $S_{mom.i}^c$, can take values of the same order as the magnitude of the convection term and the diffusion term, which caused stability problems. Therefore, in the simulation where $S_{mom.i}^c$ is applied at the wall-parallel interface, the commutation term in the momentum equations has been limited to the minimum of the magnitude of the convection and diffusion terms as follows

$$\left(S_{mom,i}^c\right)_{lim} = \texttt{sign}\left(S_{mom,i}^c\right) \cdot \min\left\{\texttt{abs}\left(S_{mom,i}^c\right),\ \min\left[\texttt{abs}\left(C_{mom,i}\right),\ \texttt{abs}\left(D_{mom,i}\right)\right]\right\} \tag{24}$$

where

$$C_{mom,i} = \overline{u}_j \frac{\partial \overline{u}_i}{\partial x_j} \tag{25}$$

$$D_{mom,i} = \frac{\partial \tau_{ij}}{\partial x_j}, \qquad \tau_{ij} = (\nu_t + \nu)\left(\frac{\partial \overline{u}_i}{\partial x_j} + \frac{\partial \overline{u}_j}{\partial x_i}\right) \tag{26}$$

The applied source term is often limited by Eq. (24). Moreover, the source term $S_{mom,i}^c$ fluctuates stongly and is limited both by $\texttt{abs}\,(C_{mom,i})$ and $\texttt{abs}\,(D_{mom,i})$. Due to the limitation of this source term, the effect of the term at the wall-parallel RANS-LES interface is small as seen in Section 3 in both the channel flow simulations and in the simulations of the spatially developing boundary layer.

Note that the terms S_k^c and $S_{mom,i}^c$ are added to the instantaneous flow field and the addition of the terms according to strategy 1 to 3 in Fig. 2 is determined by the instantaneous velocity orthogonal to the interface, v_{int}. Hence, even though the time-averaged v_{int} is zero, S_k^c and $S_{mom,i}^c$ will have an effect on the mean flow field. However, the effect of these terms are smaller for a mean flow aligned with the RANS-LES interface compared to a mean flow across an interface as the wall-normal interface described above.

2.4 Synthetic turbulent fluctuations

Synthetic turbulent fluctuations are superimposed onto the RANS mean flow field at the wall-normal interface or inlet in the simulations of channel flow and boundary layer flow as given in Table 1. Anisotropic STF, based on a modified von Karman spectrum, are used. The methodology to generate the STF is presented in the work by Davidson [21, 16] and Davidson and Peng [22].

Two different approaches have been used to apply the STF in the simulations. When the STF are applied at the inlet boundary, as in the boundary layer simulations, the STF are added directly to the mean velocities in the inlet boundary condition. In the channel flow simulations where STF are applied to the embedded wall-normal interface the STF are applied as source terms in the momentum equations.

The procedure for generating the STF is summarized below.

- A precursor RANS simulation is made using the PDH-LRN model [18] in order to get profiles of u, k and ω at the inlet for the simulations of boundary layer flow and upstream of the embedded interface for the simulations of channel flow.
- The RANS profiles are used as input to compute the Reynolds stress tensor according to the Wallin and Johansson EARSM model [23].
- The Reynolds stress tensor and the turbulent length scale $l_{t,s}$ are used as input for the generation of the anisotropic homogeneous turbulence.
- Since the synthetic turbulence that is generated is homogeneous, the Reynolds stress tensor can only be applied in one point. The shear stress is the most important stress component in attached boundary layer flows; we therefore choose the point where the turbulent shear stress is largest.

- As a last step, the turbulent fluctuations are scaled with $\left(\left|\overline{u'v'}\right| / \left|\overline{u'v'}\right|_{\max}\right)^{1/2}_{RANS}$, which is taken from the precursor RANS simulation.

Synthetic turbulent fluctuations applied to the simulations of channel flow and boundary layer flow are shown in Fig. (3).

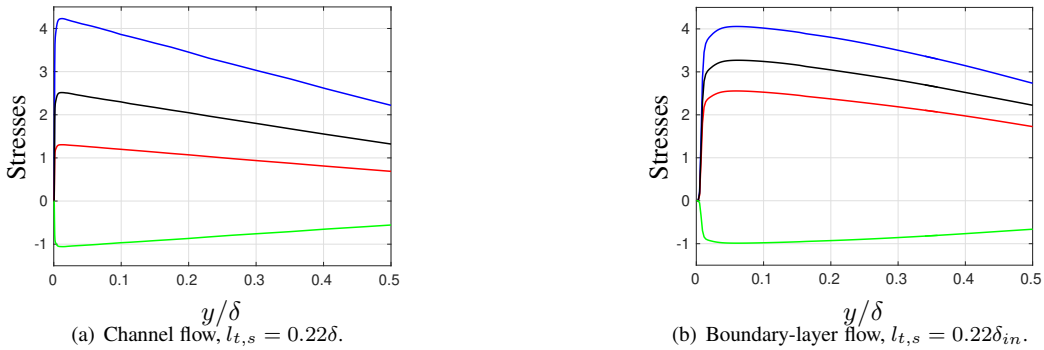

(a) Channel flow, $l_{t,s} = 0.22\delta$.

(b) Boundary-layer flow, $l_{t,s} = 0.22\delta_{in}$.

Figure 3: Synthetic turbulent stresses applied at the embedded interface in simulations of channel flow and at the inlet in simulations of boundary layer flow. Subscript s denotes synthetic. —: $\langle u'_s u'_s \rangle^+$; —: $\langle v'_s v'_s \rangle^+$; —: $\langle w'_s w'_s \rangle^+$; —: $\langle u'_s v'_s \rangle^+$.

The difference observed between the synthetic turbulent fluctuations applied in simulations of channel flow and boundary layer flow is due to differences in the RANS shear stress profiles and the Reynolds stress tensors from the EARSM. Since the commutation terms in the k and ω equations are applied in the near-wall RANS region at the inlet (boundary layer flow) and the embedded interface (channel flow), the synthetic fluctuations are applied in this region too.

To compute the turbulent time scale needed for the time correlation for the used synthetic turbulent fluctuations as described in [21], the bulk velocity and the turbulent length scale $l_{t,s}$ are used. Thus, no additional parameters are needed than those described above. It should be noted that, with the commutation terms combined with the procedure described for generating STF, the only "free" parameter in the RANS-LES interface method used is the turbulent length scale.

3 Results and discussion

In the simulation strategy used in the present paper, the proposed source terms are applied at both the wall-parallel RANS-LES interface and the wall-normal interface. At the inlet and at the embedded interface, respectively, in the simulations of boundary layer flow and channel flow, synthetic turbulent fluctuations are superimposed onto the mean flow. Since the change in modeled turbulent kinetic energy from RANS to LES at the inlet and across the wall normal embedded interface is compensated by the addition of synthetic turbulence, no commutation terms are added in the momentum equations. Only the commutation terms in the k and ω equations are applied at the interface, in order to achieve a reduction of the modeled turbulent kinetic energy (and the turbulent viscosity) from the RANS side to the LES side of the interface.

No additional synthetic turbulence is added to the mean flow at the RANS-LES interface in the simulations of the mixing layer; instead the commutation terms in the momentum equations are added to compensate for the reduction in modeled turbulent kinetic energy due to the commutation terms in the k and ω equations.

In simulations where wall-parallel interfaces are present, source terms in k, ω and momentum equations are applied at these interfaces. In all results presented below, $\langle \cdot \rangle$ means averaging in time and in the spanwise z direction.

3.1 Channel flow using embedded LES

Channel flow at $Re_\tau = u_\tau \delta/\nu = 8000$ was simulated using embedded LES. As seen in Fig. 4, the flow is simulated with RANS upstream of the embedded wall-normal interface. At the interface, the simulation is switched from RANS to embedded LES. In the embedded LES region, the-near wall flow is simulated in RANS mode and the off-wall flow is simulated using LES. The wall-parallel interface is prescribed at $y^+_{int} = 270$ and 550 which corresponds to $y_{int}/\delta = 0.034$ and 0.069, respectively, where δ is the boundary layer thickness. $\Delta = \Delta_{dw}$ is used as the LES length scale (see Eq. (8)).

Two computational domains were used with different streamwise lengths, $l_x/\delta = 12.8$ and 25.6, respectively. The dimensions of the domain cross sections are $(l_y, l_z)/\delta = (2, 1.6)$ with $(n_y, n_z) = (96, 64)$ cells. $n_x = 256$ and 512

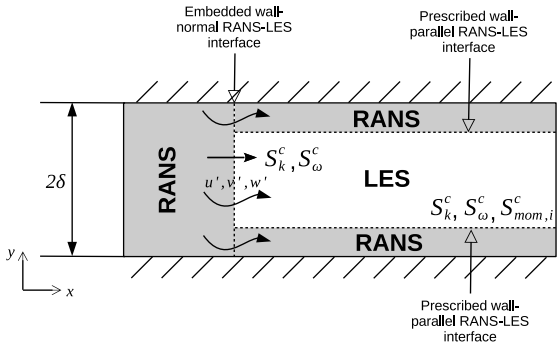

Figure 4: Channel flow. Computational domain with interfaces.

cells were used in the streamwise direction, respectively. Expressed in viscous units the grids read $(\Delta x^+, \Delta y^+, \Delta z^+) = (400, 0.7 - 980, 200)$.

Profiles of u, k and ω, from a precursor PDH-LRN RANS simulation of fully developed channel flow at $Re_\tau = 8000$, are applied at the inlet. The proposed commutation terms in the k and ω equations are introduced at the embedded wall-normal interface, located at $x/\delta = 0.925$ ($i = 20$). To get a rapid development of the LES simulated flow downstream of the interface, synthetic turbulent fluctuations are superimposed onto the mean flow field, as described in Section 2.4. Three different turbulent length scales were evaluated for the generation of the STF; $l_{t,s}/\delta = 0.15$, 0.22 and 0.30. The turbulent length scale $l_{t,s}/\delta = 0.22$ is used as reference in this work. The effect of $l_{t,s}$ and the location of the wall-parallel RANS-LES interface is discussed at the end of this section.

The commutation terms in the k, ω and momentum equations are introduced at the wall-parallel interfaces. As a reference, a simulation is used in which no commutation terms are applied at the wall-normal and the wall-parallel interfaces.

A second order upwind scheme is applied in the RANS region upstream of the embedded wall normal interface for the discretization of the momentum equations. In the region downstream of the wall normal interface, a second order central differentiating scheme is used in the LES region and the near-wall RANS regions.

The computed channel flow cases are summarized in Table 2. Case 6 was used with the aim to reach a fully developed channel flow. As seen in Fig. 5 (a), the flow is almost fully developed but an even longer domain is needed to reach a fully developed flow. On the other hand, a fully developed flow is not needed for evaluation of the wall-normal and wall-parallel RANS-LES interface methods applied with regard to grey-area mitigation and reduction of the log-layer mismatch. The small domain is used in the analysis below.

Table 2: Commutation terms applied at RANS-LES interfaces in channel flow.

Case	Wall-normal interface	Wall-parallel interface	Side of wall-parallel interface	y^+_{int}	y_{int}/δ	L_x/δ	$l_{t,s}/\delta$
1	None	None	N/A	550	0.069	12.8	0.22
2a	k, ω	None	N/A	550	0.069	12.8	0.15
2b	k, ω	None	N/A	550	0.069	12.8	0.22
2c	k, ω	None	N/A	550	0.069	12.8	0.30
2d	k, ω	None	N/A	270	0.034	12.8	0.22
3	k, ω	k, ω	LES	550	0.069	12.8	0.22
4	k, ω	k, ω	RANS & LES	550	0.069	12.8	0.22
5a	k, ω	k, ω, u, v, w	LES	550	0.069	12.8	0.22
5b	k, ω	k, ω, u, v, w	LES	270	0.034	12.8	0.22
6	k, ω	None	N/A	550	0.069	25.6	0.22

The impact of the commutation terms and the synthetic turbulent fluctuations at the wall-normal interface is strong, as shown in Fig. 5. A quick reduction of the turbulent viscosity is obtained across the interface due to the commutation terms, and a rapid growth of the resolved turbulent stresses, are given for the downstream flow due to the synthetic turbulence.

The difference seen in the friction velocity (Fig. 5 (a)) between the reference simulation and the simulations where commutation terms are added at the wall-normal interface is of the same magnitude as the differences between the simu-

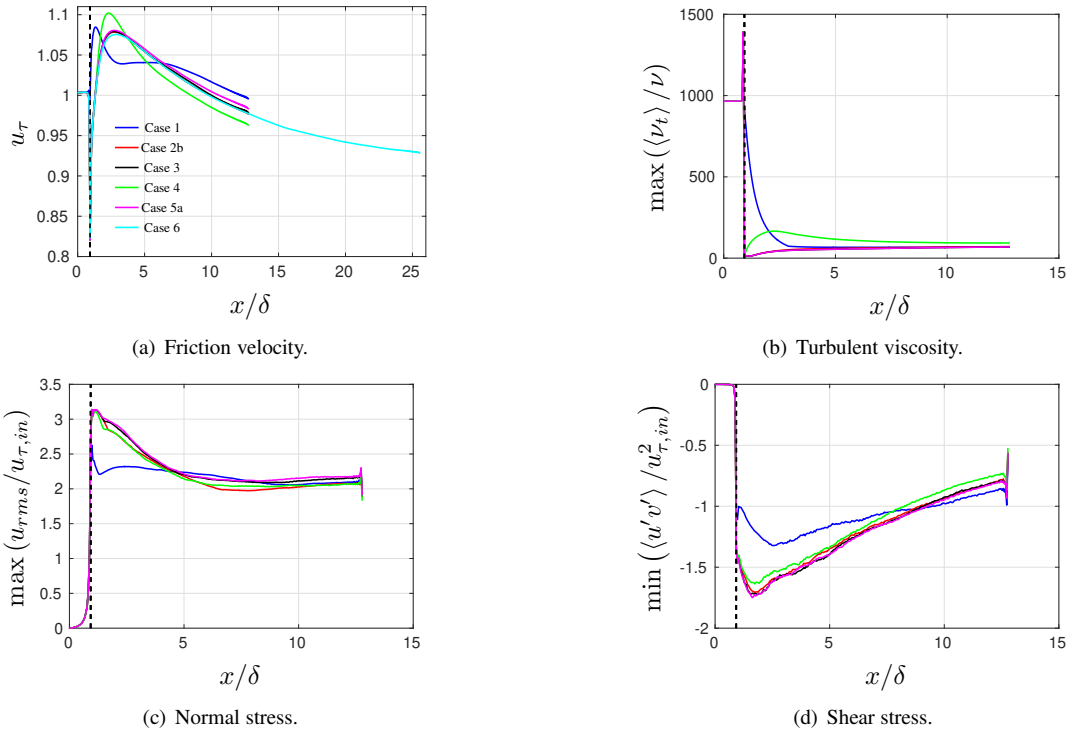

(a) Friction velocity.

(b) Turbulent viscosity.

(c) Normal stress.

(d) Shear stress.

Figure 5: Channel flow. Effect of embedded wall-normal RANS-LES interface. Colors in (a) apply for all sub-figures. Vertical dashed black line indicates wall-normal interface.

lations where commutation terms are added at the wall-parallel interfaces. Downstream of $x/\delta \simeq 7$, the friction velocity has almost the same slope in all simulations. However, none of the simulations have reached a fully developed state within the simulated channel length.

The channel flow simulated in this work should not be mixed up with fully developed channel flow. In fully developed channel flow, periodic boundary conditions are used and the driving pressure gradient balances the wall shear stress, i.e. $u_\tau = 1$. In the channel flow simulated in this work the mass flow rate is prescribed from the upstream RANS region and the wall-shear stress does not necessarily balance the driving pressure gradient since the hybrid RANS-LES velocity profile does not fully capture the inlet RANS velocity profile. Thus, the only way to compensate for this difference is through a change in the friction velocity. With the simulation approach used in this work this can be summarized as

$$\int_{inlet} \rho U^2 dy \neq \int_{outlet} \rho U^2 dy \tag{27}$$

since the velocity profile changes between the inlet and the outlet, mainly because the velocity profiles predicted by the RANS and hybrid RANS-LES are different, which gives that $u_\tau < 1$ when $x \to \infty$. Moreover, the different interface methods used gives different hybrid RANS-LES predicted velocity profiles. Hence, the right hand side of Eq. (27) will differ between the simulated cases and thus give the different friction velocity levels seen in Fig. 5 (a).

The use of the commutation terms in the k and ω equations on both sides of the wall-parallel interface gives a quicker growth of the maximum turbulent viscosity downstream of the wall-normal interface compared to the simulations where no commutation terms are applied at the wall-parallel interfaces or where the commutation terms are applied only on the LES side. Due to the higher turbulent viscosity on the LES side of the interface, a slightly lower magnitude of the maximum shear stress is obtained, as shown in Fig. 5.

The commutation term is compared to the production term, P^k, in the k equation at the wall-normal and wall-parallel interfaces, in Fig. 6. The commutation term at the wall-normal interface is stronger than the commutation term added at the wall-parallel interfaces. Except at the peak of the production term in the k equation, the commutation term at the wall-normal interface is as large as ten to 15 times the production term, which explains the strong reduction of the turbulent viscosity across the interface. Moreover, a much reduced magnitude of the production term in the k equation is observed when the commutation terms in the k and ω equations are applied at the wall-normal interface than in the reference simulation, where no commutation terms are applied. The small peaks observed in the commutation term at the wall-normal interface at $y^+ = 550$ are a consequence of the commutation terms applied at the wall-parallel interface.

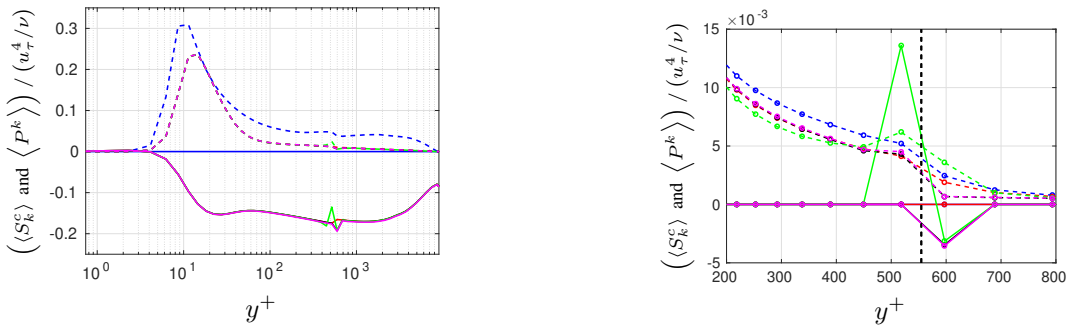

(a) At the interface, $x/\delta = 0.925$.

(b) At $x/\delta = 5.025$.

Figure 6: Channel flow. Commutation (solid) and production (dashed) terms in the k equation. In (a), the lines representing simulations with the commutation terms applied in the k, ω (Case 3) and momentum equations (Case 5a) overlap. Markers indicate cell centers of the grid. Vertical dashed black line indicates wall-parallel interface. Colors as in Fig. 5.

The effect of the commutation terms across the wall-normal interface at $y^+ = 120$ ($y/\delta = 0.015$) on the terms in the k equation is shown in Fig. 7 (a). It is observed that the commutation term is dominating over the production, dissipation and the diffusion terms at the wall-normal interface. Since the commutation term is only applied at the wall-normal interface for the shown y^+-value, the commutation term is zero elsewhere. The strongest effect is given on the production and dissipation terms while the effect on the diffusion term is small for this location at the wall-normal interface. The peak in the production term at the adjacent node upstream of the wall-normal interface is due to the STF added.

Across the wall-parallel interface, which is shown in Fig. 7 (b)-(d), it is observed that the diffusion term is most affected by the introduction of the commutation terms in Case 4, where commutation terms in the k and ω equations are added on both sides on the wall-parallel interface. However, for Case 3 the effect on the diffusion term is almost negligible. Moreover, the commutation term in the k equation is of the same magnitude as the production term as well as the diffusion and dissipation terms. Hence, the commutation term has a strong effect on the balance between the different terms in k-equation at the RANS-LES interface. Although not shown here, the effect on the terms in the k equation due to the commutation term in the momentum equation is almost negligible. Furthermore, it is observed that the magnitude of the commutation term on the RANS side of the wall-parallel interface is larger than on the LES side, as they should according to Section 2.3.2.

For the reference simulation (Case 1), where no commutation terms have been applied at the wall-normal interface, a slower reduction of the turbulent viscosity downstream of the interface is observed in Fig. 5. Moreover, the slower reduction of ν_t prevents the resolved turbulent stresses from reaching levels as high as in the interface region as in the simulations, where the commutation terms in the k and ω equations are applied.

It is observed that the reference simulation gives the lowest value of the maximum resolved shear stress, but the largest friction velocity, shortly downstream of the wall-normal interface. However, as seen in Fig. 8 (b), the near-wall total turbulent shear stress is larger in the reference simulation than in the other simulations presented in this region. The low levels of resolved shear stress is also reflected in the resolved turbulent kinetic energy for Case 1 as seen in Fig. 8 (c). On the RANS side, close to the wall-parallel interface, the modeled turbulent kinetic is almost twice as high for Case 1 compared to the other simulations. Moreover, it is observed that the low level of turbulent viscosity shortly downstream of the wall-normal interface, given by the commutation terms in the k and ω equations, in combination with the added STF stimulates the equations to resolve the turbulence and hence give the high resolved part of the turbulent kinetic energy as seen for Case 2b to 5a.

The turbulent viscosity, the turbulent shear stress and the turbulent kinetic energy at $x/\delta = 5.025$ are presented in Fig. 9. When the commutation terms in the k and ω equations are also applied on the RANS side of the wall-parallel interface, the magnitude of the turbulent viscosity is doubled compared to the other simulations. This is also reflected in the shear stress and the turbulent kinetic energy. The growth of the resolved shear stress as well as the resolved turbulent kinetic energy in the wall-normal direction is weaker when the commutation terms are applied on both sides of the interface. However, the peak of the shear stress and the resolved turbulent kinetic energy is almost as high and in the same location as for the other cases.

Velocity profiles are given in Fig. 9 (a). It is observed that the log-layer mismatch is almost negligible at this location. This is due to the STF added on the upstream wall-normal RANS-LES interface which stimulates the flow in the region of the wall-parallel interface to quickly develop a turbulence resolving flow on the LES side of the interface. However, the further downstream of the wall-normal RANS-LES interface the velocity is evaluated, i.e. closer to fully developed flow,

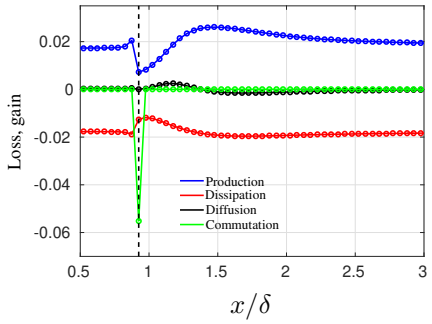

(a) Case 2b: at wall-normal interface.

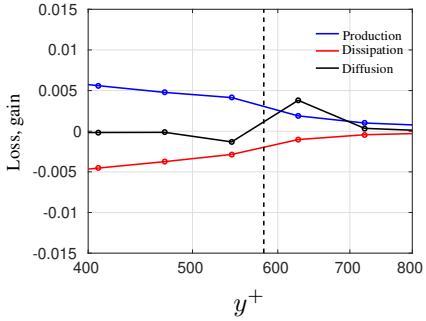

(b) Case 2b: at wall-parallel interface.

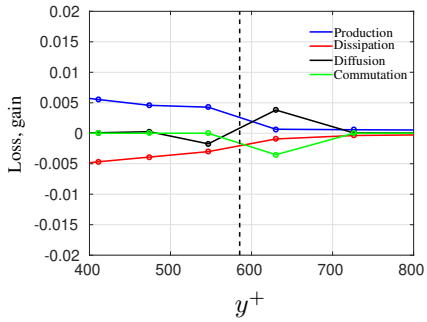

(c) Case 3: at wall-parallel interface.

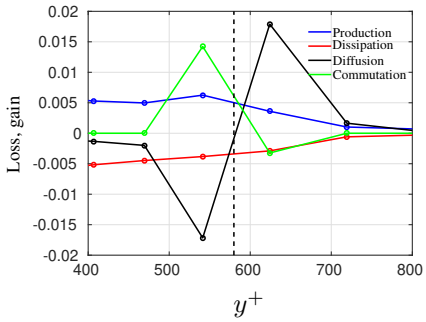

(d) Case 4: at wall-parallel interface.

Figure 7: Channel flow. Budgets for the modeled turbulent kinetic energy equation. (a) Data at $y^+ = 120$ ($y/\delta = 0.015$). (b)-(d) Data at $x/\delta = 5.025$. Terms scaled with u_τ^4/ν. Markers indicate grid cell centers. Vertical dashed black line indicate RANS-LES interfaces.

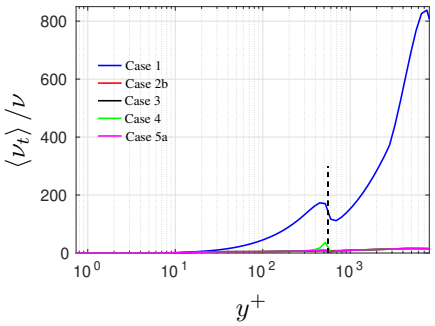

(a) Turbulent viscosity.

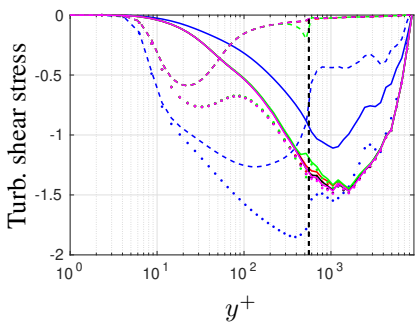

(b) Shear stress.

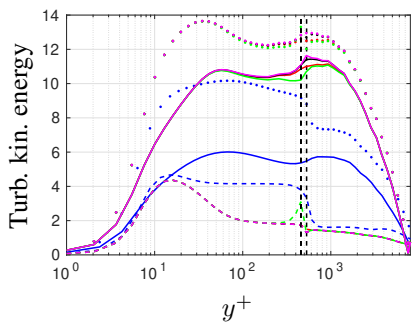

(c) Turbulent kinetic energy.

Figure 8: Channel flow. Turbulent viscosity and shear stress at the downstream cell adjacent to the wall-normal interface ($i = 21$), $x/\delta = 0.9750$. (b) Resolved (solid), modeled (dashed) and total (dotted) turbulent kinetic energy. (c) Resolved (solid), modeled (dashed) and total (dotted) shear stress. Vertical dashed black line indicates wall-parallel interface.

the stronger the effect on the log-layer mismatch due to the different wall-parallel RANS-LES interface methods. It was concluded in Arvidson et al. [24] that for fully developed channel flow, strategy 2 for wall-parallel RANS-LES interfaces appears to be the worst from a log-layer mismatch perspective while strategies 1 and 3 give similar results with a much reduced log-layer mismatch. It should however be noted that the LES length scale $\Delta = \Delta_{dw}$ itself almost eliminates the log-layer mismatch compared to e.g. $\Delta = \Delta_{max}$ and that the effect on the log-layer mismatch due to the different wall-parallel interface strategies are small. Especially between strategy 1 and 3.

The turbulent viscosity for the simulation where the commutation terms in the k and ω equations are applied on the LES side of the wall-parallel interface coincides with the simulation where the commutation terms are also applied in the momentum equations. These two simulations give the lowest level of turbulent viscosity. This is expected since the commutation terms in the k and ω equations are applied only on the LES side of the interface with the aim to reduce the turbulent viscosity. Moreover, it is observed that the highest shear stress peak is obtained when the commutation terms

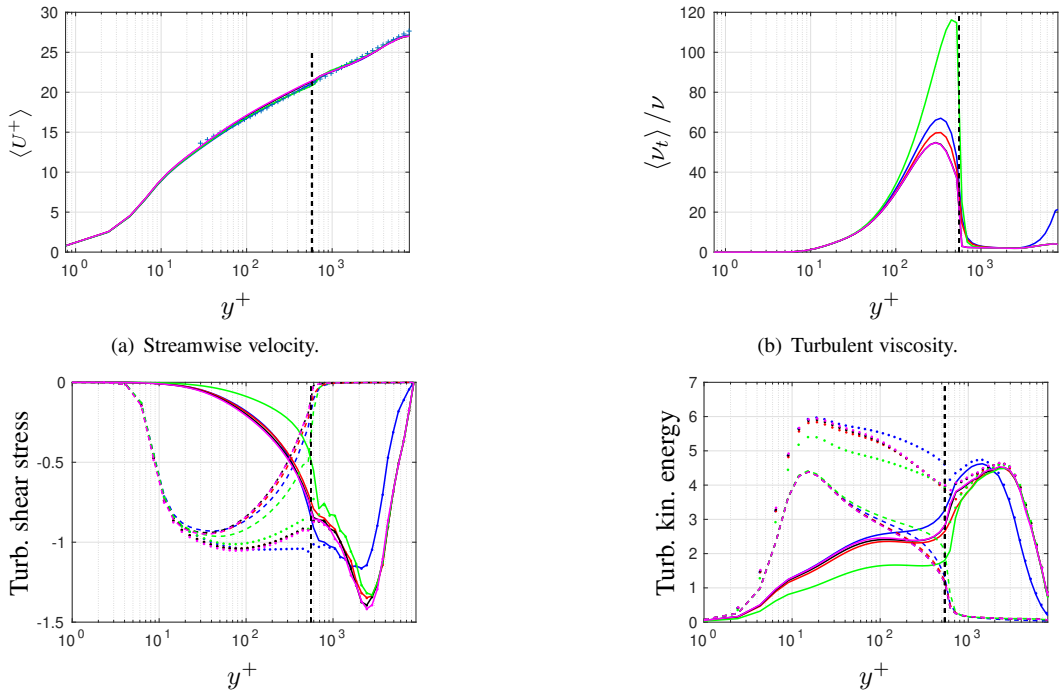

(a) Streamwise velocity. (b) Turbulent viscosity. (c) Shear stress. (d) Turbulent kinetic energy.

Figure 9: Channel flow. (a) Streamwise velocity. (b) Turbulent viscosity. (c) Resolved (solid), modeled (dashed) and total (dotted) shear stress. (d) Resolved (solid), modeled (dashed) and total (dotted) turbulent kinetic energy. Vertical dashed black line indicates wall-parallel interface. Data at $x/\delta = 5.025$.

are also applied to the momentum equations.

The effect of the location of the wall-parallel RANS-LES interface as well as the turbulent length scale, $l_{t,s}$, used in the generation of STG are evaluated in Figs. 10 and 11. The effect of the location of the wall-parallel interface is given by comparing Case 2b and 2d as well as 5a and 5b, where Cases 5a and 5b have used strategy 3, see Fig. 2. In Cases 2a-d no commutation terms are applied at the wall-parallel RANS-LES interface. The effect of different $l_{t,s}$ is given by the comparison of Case 2a, 2b and 2c. Case 2b and 5a are included as references.

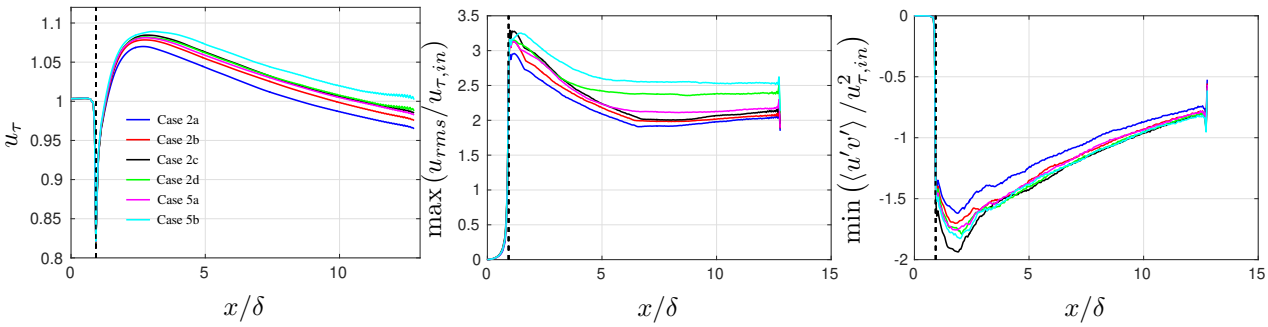

(a) Friction velocity. (b) Normal stress. (c) Shear stress.

Figure 10: Channel flow. Effect of turbulent length scale used in the generation of synthetic turbulent fluctuations at the wall-normal interface. Data along x-direction. Vertical dashed black line indicates wall-normal interface.

By comparing Figs. 5 and 10 it is concluded that the effect of the variation of $l_{t,s}$ used in the generation of the STG and different wall-parallel interface locations is of the same order as applying the different strategies for the wall-parallel RANS-LES interface as proposed in Section 2.3.2. Although not shown here, this includes also the log-layer mismatch for the velocity profiles.

The wall-parallel RANS-LES interface location (Case 2d and 5b) gives a stronger effect on the flow downstream of the wall-normal interface compared to the change in the turbulent length scale used in the generation of the STF. The wall-

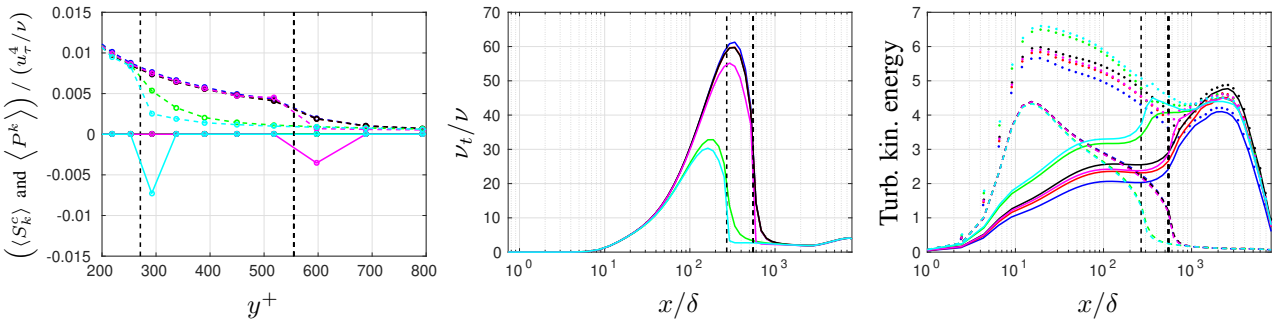

(a) Commutation term. (b) Turbulent viscosity. (c) Turbulent kinetic energy.

Figure 11: Channel flow. Effect of turbulent length scale used in the generation of synthetic turbulent fluctuations at the wall-normal interface. Data at wall-parallel RANS-LES interfaces at $x/\delta = 5.025$. (a) Commutation term (solid lines) and production term (dashed lines) in k equation. (b) Turbulent viscosity. Case 2b ans 2c overlap. (c) Resolved (solid lines), modeled (dashed lines) and total (dotted lines) turbulent kinetic energy. Colors as in Fig. 10. Vertical dashed black lines indicate wall-parallel interfaces.

parallel interface location closer to the wall gives a lower peak value of the turbulent viscosity as expected and a more rapid growth of the shear stress in the wall-normal direction as seen in Fig. 11. However, the effect of the wall-parallel interface location on the peak value of the shear stress is almost negligible, especially far downstream of the wall-normal RANS-LES interface as seen in Fig. 10 (c). This is also reflected in the velocity profiles where it is observed that the difference in the log-layer mismatch between the two interface locations for the simulated cases are almost negligible (not shown).

A larger difference is observed in the peak of the normal stress with respect to the location of the wall-parallel interface as seen in Fig. 10 (b). The effect of using the commutation terms in k, ω and momentum equations (strategy 3) compared to no commutation terms at the wall-parallel RANS-LES interface is stronger when the interface is located closer to the wall. The reason is that the commutation term in the k equation (S_k^c) takes a higher value as seen in Fig. 11 (a). As a consequence of the higher value of S_k^c, the commutation term in the momentum equation $S_{mom,i}^c$ also get stronger since S_k^c is included in this term (Eq. 20). Moreover, with the wall-parallel interface closer to the wall, the fluctuations u', v' and w' get stronger in the near-wall region (not shown here) which further amplifies the effect of $S_{mom,i}^c$.

3.2 Spatially developing boundary layer

Spatially developing turbulent boundary layer is simulated using embedded LES, as shown in Fig. 12. The Reynolds number range covered by the simulations is $3025 \leq Re_\theta = U_{inf}\theta/\nu \leq 5700$, where θ is the momentum thickness and $U_{inf} = 70$ m/s is the freestream velocity. The Reynolds number range based on the friction velocity u_τ and the boundary layer thickness δ is $1170 \leq Re_\theta = u_\tau\delta/\nu \leq 2145$.

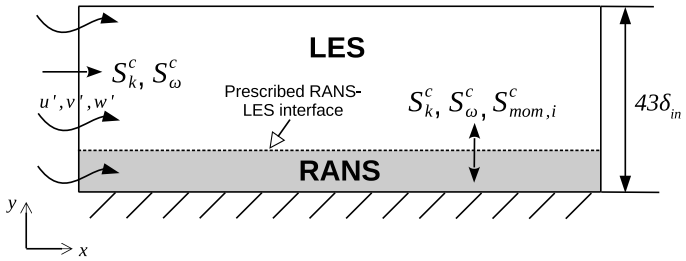

Figure 12: Boundary layer. Computational domain with interfaces.

Profiles of u, v, k and ω, from a precursor RANS simulation using the PDH-LRN model [18], are prescribed at the inlet boundary. The RANS values of the turbulent kinetic energy and the specific dissipation rate of k are manipulated using the commutation terms in the k and ω equations, as described in Section 2.3.2, in order to reach typical LES levels. Synthetic turbulent fluctuations are imposed at the inlet boundary to get a rapid evolvement of the downstream turbulence resolving LES flow. The flow is simulated with a near-wall RANS layer and an off-wall LES region. The wall-parallel

RANS-LES interface is located at $y^+ = 220$. Expressed in fraction of the boundary layer the wall-parallel switch is located at $y_{int}/\delta = 0.096$ to 0.190 depending on the x-location. The proposed commutation terms in the k, ω and momentum equations are evaluated at the RANS-LES interfaces. The LES length scale $\Delta = \Delta_{dw}$ is used (see Eq. (8)). As spatial discretization of the momentum equations, a second order central differentiating scheme is used in both the RANS and LES regions.

The dimensions of the grid used are, $(L_x, L_y, L_z)/\delta_{in} = (85, 43, 2.93)$ and consists of $(n_x, n_y, n_z) = (872, 124, 60)$ cells. The grid reads in viscous units $(\Delta x^+, \Delta y^+, \Delta z^+) = (104, 1 - 3688, 52)$. Data from the simulations are compared to DNS data by Schlatter and Örlü [25] at $Re_\theta = 4060$ and experimental data by DeGraaff and Eaton [26] at $Re_\theta = 5200$, which correspond to simulated streamwise distances of $x/\delta_{in} = 24$ and $x/\delta_{in} = 56$, respectively. The parameter that is the most important to capture in the boundary layer simulations presented is the skin friction. As reference for the skin friction, the Coles-Fernholz correlation is used. The simulated flow cases are summarized in Table 3. The topology of the imposed synthetic turbulence at the inlet and resolved turbulent structures along the spatially developing boundary layer for case 2 are given in Fig. 13.

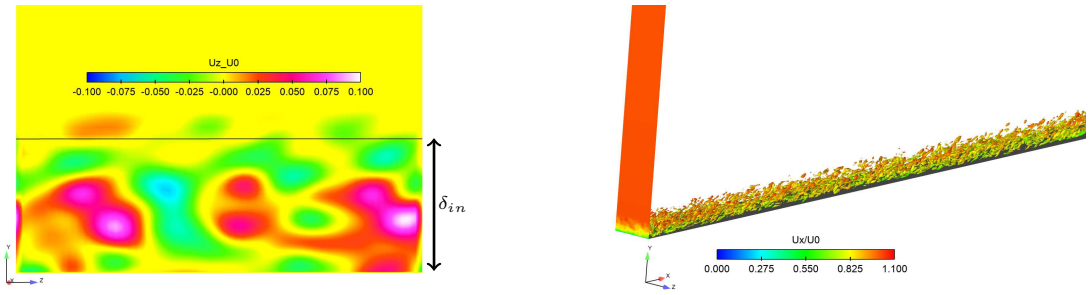

(a) Imposed turbulent structures at inlet. Colors shows instantaneous spanwise velocity fluctuations.

(b) Resolved turbulent structures. Colors shows instantaneous streamwise velocity.

Figure 13: Boundary layer. Flow topology for case 2. (a) Topology of imposed synthetic turbulence at inlet. (b) Resolved turbulent structures visualized as Q-criterion, $Q\left(\delta_{in}/U_{\text{inf}}\right)^2 = 0.075$, along the simulated spatially boundary layer.

Table 3: Commutation terms applied at RANS-LES interfaces in boundary layer flow.

Case	Wall-normal interface	Wall-parallel interface	Side of wall-parallel interface
1	None	None	N/A
2	k, ω	None	N/A
3	k, ω	k, ω	LES
4	k, ω	k, ω	RANS & LES
5	k, ω	k, ω, u, v, w	LES

It should be noted that the PDH-LRN RANS model does not predict a proper relationship between the skin friction coefficient (C_f) and the momentum thickness (θ) for the spatially developing boundary layer flow that is simulated. To achieve a correct relationship between C_f and θ at the inlet, Direct Numerical Simulation (DNS) data or correlations for the inlet streamwise velocity profile can be used, e.g. as in Davidson [19]. However, in this paper the PDH-LRN RANS velocity profile is used at the inlet since this simulation procedure is more relevant for industrial applications.

The skin friction distribution and the maximum turbulent viscosity are presented in Fig. 14. The commutation terms, in the k and ω equations, applied at the inlet strongly affects the turbulent viscosity as also observed in the channel flow simulations. Moreover, the addition of the synthetic turbulent fluctuations at the inlet gives a rapid growth of the turbulent stresses (not shown) and an over-prediction of the skin friction, due to an over-estimation of the near-wall shear stress shortly downstream of the inlet.

The behavior of the commutation term in the k equation, as shown in Fig. 15, is similar to the behavior observed at the RANS-LES interfaces in simulations of channel flow. The commutation term is much larger than the production term at the inlet but the two terms are of the same magnitude at the wall-parallel interface. The commutation term at the wall-parallel RANS-LES interface in boundary layer flow is of the same magnitude as the dissipation and diffusion terms

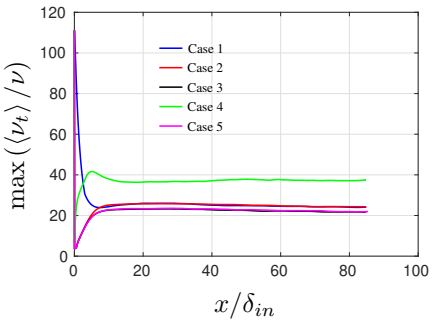

(a) Turbulent viscosity.

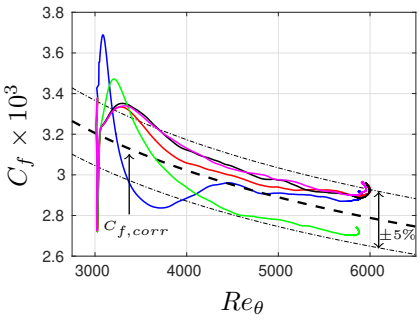

(b) Skin friction.

Figure 14: Boundary layer. Maximum turbulent viscosity and skin-friction coefficient. In (b) $C_{f,corr} = 2\left(\frac{1}{0.384}\ln(Re_\theta) + 4.127\right)^{-2}$.

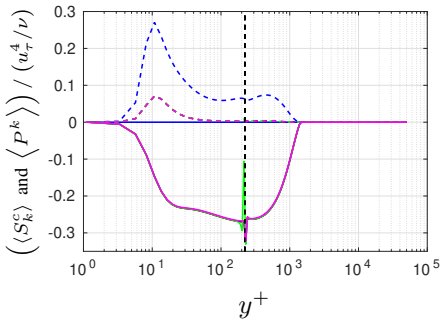

(a) Cell layer adjacent to the inlet.

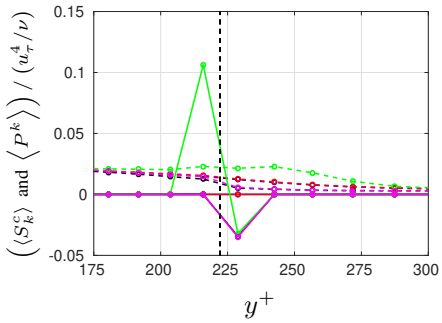

(b) $Re_\theta = 5200$

Figure 15: Boundary layer. Commutation (solid) and production (dashed) terms in the k equation. Vertical dashed black line indicates the wall-parallel interface. Markers indicate grid cell centers. In (a), the lines representing simulations with the commutation terms applied in the k, ω (Case 3) and momentum equations (Case 5) overlap. Colors as in Fig. 14.

(not shown here) and hence affect the balance between these terms as in the channel flow simulations. It is noted that the commutation term in the momentum equations has a negligible effect on the commutation term in the k equation due to the limitation by Eq. (24). In addition, the turbulent viscosity in these two simulations is similar.

The use of different RANS-LES interface methodologies are clearly observed in the predicted skin friction distributions. The most rapid recovery of the flow to a fully developed state is given when the commutation terms in the k and ω equations are applied at the inlet, and when either no treatment of the wall-parallel interface is applied or the commutation terms in the k and ω equations are applied only on the LES side of the interface. The flow in these simulations is fully recovered at $x/\delta_{in} \simeq 23$ ($Re_\theta \simeq 4000$). The recovery obtained with the commutation terms added in the momentum equations is similar to the case where the commutation terms are added in the k and ω equations. The weak effect of the terms in the momentum equations is due to the limitation of these terms as described above. A slower recovery is obtained if the commutation terms in the k and ω equations are added on both the RANS and LES sides of the wall-parallel interface. This simulation predicts a fully developed flow at $x/\delta_{in} \simeq 39$ ($Re_\theta \simeq 4600$). However, it is important to highlight that all boundary layer simulations presented are within $\pm 5\%$ from the used reference correlation.

It is observed that Case 4 in the boundary layer simulations, where strategy 2 (see Fig. 2 (b)) is used for the wall-parallel RANS-LES interface, is more sensitive to the high level of turbulent viscosity at the RANS-LES interface compared to the corresponding case in the channel flow simulations (case 4). The effect of switch location using strategy 2 was evaluated for fully developed channel flow at $Re_\tau = 8000$ in Arvidson et al. [24] with the conclusion that the log-layer mismatch, and thus also the change in skin friction (or friction velocity), is amplified the farther from the wall the RANS-LES switch is located. With strategy 1 and 3 this was not the case. In the channel flow simulations using strategy 2 in this work the switch is located at $y_{int}/\delta = 0.069$ ($y^+_{int} = 550$) and in the boundary layer flow at $y_{int}/\delta = 0.096$ to 0.190 ($y^+_{int} \approx 220$) depending on the x-location. Since the switch location in the simulated boundary layer flow is located farther away from the wall (measured as fraction of the boundary layer thickness, y_{int}/δ) compared to the channel flow case it is expected that the difference between case 4 and 5 should be more pronounced in the boundary layer flow than in the channel flow case.

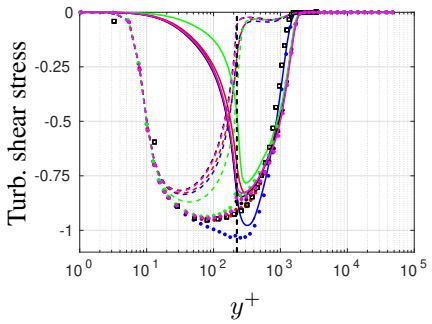

(a) $Re_\theta = 4060$.

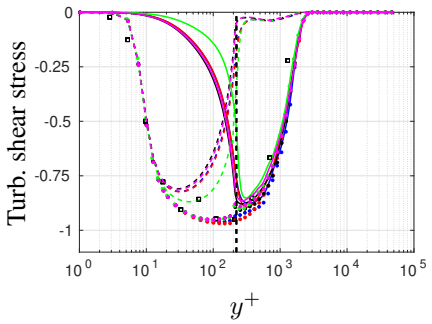

(b) $Re_\theta = 5200$.

Figure 16: Boundary layer. Turbulent shear stress. Resolved stress: solid lines; modeled stress: dashed; total stress: dotted. Markers are DNS data [25] at $Re_\theta = 4060$ and experimental data [26] at $Re_\theta = 5200$. Vertical dashed black line indicates the wall-parallel interface. Colors as in Fig. 14.

When no commutation terms are used at the inlet, the excess of turbulent viscosity shortly downstream of the interface gives a large peak in the skin friction with a subsequent rapid skin friction reduction and a slow recovery of the flow towards its fully developed state. The large turbulent viscosity close to the inlet gives an over-prediction of the shear stress, which is reflected in the skin friction. However, the high turbulent viscosity has a dampening effect on the added synthetic turbulent fluctuations. The fluctuations decay more rapidly in this simulation as compared to the simulations where commutation terms are added at the inlet (not shown). This gives a lower level of the near wall shear stress and thus an under-prediction of the skin friction. Resolved turbulence is developed further downstream, and the flow approaches a fully developed state.

The predicted shear stresses at $Re_\theta = 4060$ and 5200, respectively, agree well with the DNS and the experimental data as seen in Fig. 16. It should be noted that the largest peaks in the shear stress and the streamwise fluctuations at $Re_\theta = 4060$ are observed for the reference simulation, where no commutation terms are added at the wall-normal and the wall-parallel interfaces. At this location, all other simulations have almost reached a fully developed state but not the reference simulation. Changing the flow towards a fully developed state requires a change of the velocity profile, which has to be made through the turbulent stresses. Further downstream at $Re_\theta = 5200$, as shown in Figs. 16 and 19, all simulations presented are fully developed and the stresses are almost aligned with each other.

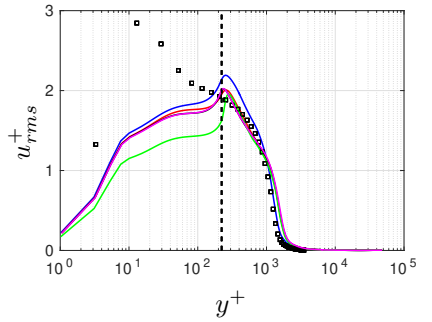

(a) $Re_\theta = 4060$.

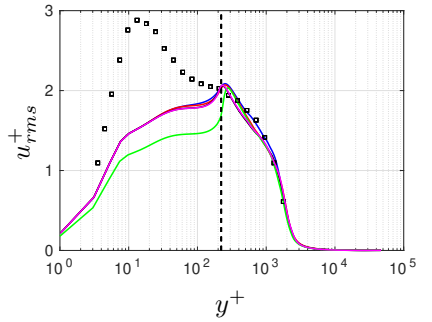

(b) $Re_\theta = 5200$.

Figure 17: Boundary layer. Resolved turbulent normal stress, $\langle u'u' \rangle$. Markers are DNS data [25] at $Re_\theta = 4060$ and experimental data [26] at $Re_\theta = 5200$. Dashed black line indicates the wall parallel interface. Colors as in Fig. 14.

The streamwise velocity profiles and the turbulent viscosity at $Re_\theta = 5200$ are shown in Fig. 20. The predicted velocity profiles are in good agreement with the experimental data. With the commutation terms applied only on the LES side a minor improvement of the log-layer mismatch is given compared to the reference simulation. The LES length scale $\Delta = \Delta_{dw}$ effectively reduces the turbulent viscosity (and the modeled turbulent kinetic energy) at the wall-parallel RANS-LES interface, hence the effect of the commutation terms should be small since the difference between k_{RANS} and k_{sgs} in Eq. (23) get small with $\Delta = \Delta_{dw}$. A slight over-prediction of the free-stream velocity is observed for the simulations where the commutation terms in the k and ω are applied on both sides of the wall-parallel RANS-LES interface. As observed in the channel flow simulations, the commutation terms applied on the RANS side of the wall-

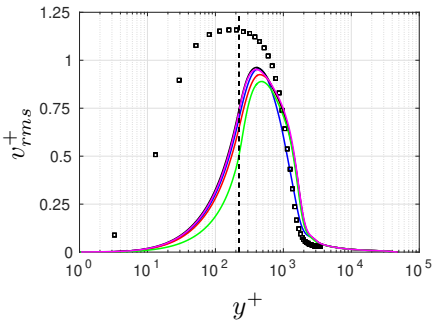

(a) $Re_\theta = 4060$.

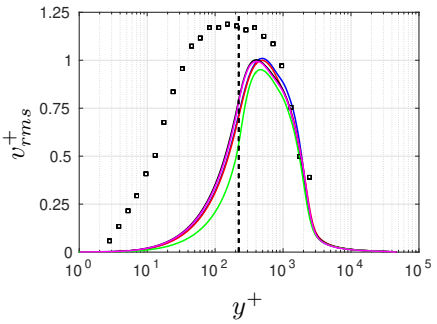

(b) $Re_\theta = 5200$.

Figure 18: Boundary layer. Resolved turbulent normal stress, $\langle v'v' \rangle$. Markers are DNS data [25] at $Re_\theta = 4060$ and experimental data [26] at $Re_\theta = 5200$. Dashed black line indicates the wall parallel interface. Colors as in Fig. 14.

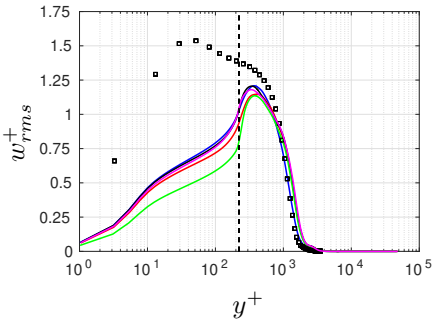

(a) $Re_\theta = 4060$.

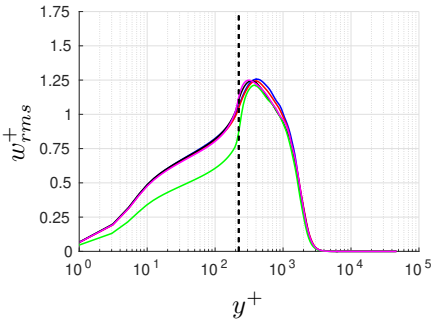

(b) $Re_\theta = 5200$.

Figure 19: Boundary layer. Resolved turbulent normal stress, $\langle w'w' \rangle$. Markers are DNS data [25]. At $Re_\theta = 5200$, no reference data is available. Dashed black line indicates the wall parallel interface. Colors as in Fig. 14.

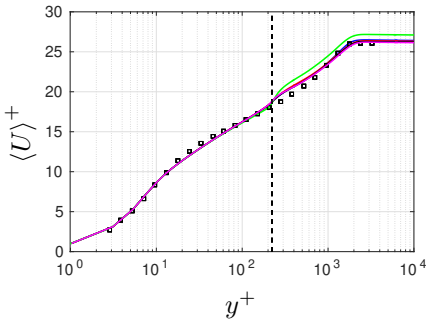

(a) Stremwise velocity.

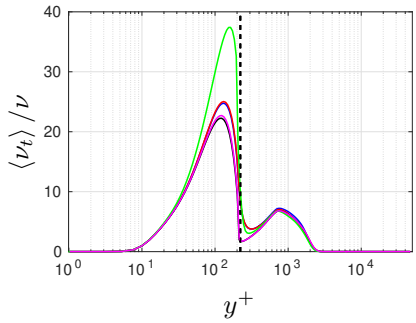

(b) Turbulent viscosity.

Figure 20: Boundary layer. Streamwise velocity and turbulent viscosity at $Re_\theta = 5200$. Markers are experimental data [26]. Dashed black line indicates the wall-parallel interface. Colors as in Fig. 14.

parallel interface have a strong effect on the turbulent viscosity and the peak is almost doubled compared to the other boundary layer simulations that are presented. This additional turbulent viscosity gives a slower development of the resolved stresses in the wall-parallel interface region, which leads to the log-layer mismatch observed at the interface.

3.3 Mixing layer

The mixing layer, investigated experimentally by Delville [27], has been simulated using an embedded LES approach as shown in Fig. 21. The computational domain includes an infinitely thin flat plate, with different boundary layers on each side, and the region downstream of the flat plate trailing edge where the two boundary layers mix. The technique used to simulate the infinitely thin flat plate was implemented in CALC-LES in Matsfelt [28]. The boundary layers on each side

of the flat plate have different freestream velocities and different Reynolds numbers. The experimental boundary layer properties at the trailing edge are presented in Table 4.

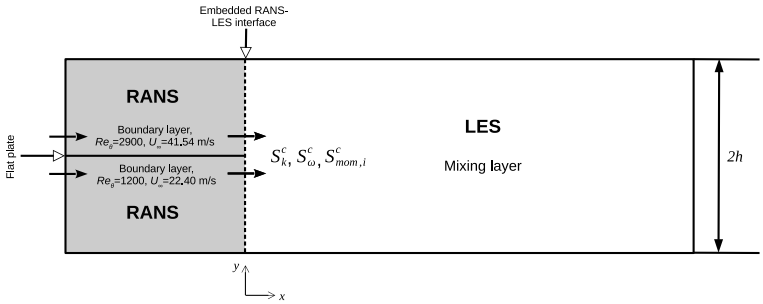

Figure 21: Mixing layer. Computational domain with embedded RANS-LES interface.

The simulated mixing layer has been numerically investigated by many research groups using different approaches in order to overcome the grey-area downstream of the flat plate trailing edge, see e.g. Kok and van der Ven [9] and Deck [29]. Some of these approaches use successfully synthetic turbulent fluctuations superimposed to the mean flow at the flat plate in order to rapidly establish a turbulence resolving flow downstream of the flat plate and hence overcome the grey-area problem. However, using synthetic turbulent fluctuations requires knowledge about the incoming flow in order to generate turbulent fluctuations with adequate spatial and temporal scales. In this work we therefore search for a generalized RANS-LES interface approach where no synthetic fluctuations are needed but the turbulence model itself generates the turbulent fluctuations needed at the interface. In this work these turbulent fluctuations are obtained by using an approach based on the commutation terms proposed in Section 2.3.

The boundary layers on each side of the flat plate are simulated with RANS. The wall-normal embedded interface, where the simulation switches from RANS to LES, is located at the trailing edge of the flat plate. The mixing layer flow downstream of the trailing edge is simulated using LES. The inlet boundary layer profiles, applied on each side of the flat plate, have been computed in separate RANS boundary layer simulations to achieve similar boundary layer profiles at the trailing edge as in the reference experiment.

Table 4: Flow conditions of the boundary layers at $x = -10$ mm. Data from experiment [27].

Measure	Notation	High velocity BL	Low velocity BL
Velocity	U_∞	41.54 m/s	22.40 m/s
Thickness	δ	9.6 mm	6.3 mm
Displacement thickness	δ_1	1.4 mm	1.0 mm
Momentum thickness	θ	1.0 mm	0.73 mm
Shape factor	H	1.35	1.37
Re-number based on θ	Re_θ	2900	1200
Turbulence level	u'/U_∞	$\sim 0.3\%$	$\sim 0.3\%$

The grids used in the simulations are based on the grid designed by NLR for the FP7 Go4Hybrid project and the Garteur AG54 project. The grid on each side of the flat plate is symmetric, with $y = 0$ located at the plate. The wall-normal grid resolves the boundary layers down to $y^+ = 1$. The flat plate has a length of 0.149 m, consisting of 20 cells in the streamwise direction, and the domain for the mixing layer downstream of the flat plate trailing edge is $L_{ref} = 1$ m. In the simulations, $x = 0$ at the trailing edge of the flat plate. The height of the domain on each side of the flat plate is $h = 0.15$ m. The spanwise extension of the domain is $z_{\max} = 0.15$ m. In the mixing layer region, the grid is equidistant in the streamwise x direction and the spanwise z direction, $\Delta x = \Delta z = 3.125$ mm for the coarse grid and $\Delta x = \Delta z = 1.5625$ mm for the fine grid. The computational domains have $(n_x, n_y, n_z) = (354, 146, 48)$ and $(n_x, n_y, n_z) = (674, 146, 96)$ cells, respectively.

Different differentiating schemes have been evaluated for the mixing layer flow as shown in Table 5. Central differentiating scheme (CDS) were evaluated for two time steps, $\Delta t = 5 \times 10^{-5}$ and 5×10^{-4} s, on the coarse grid. The smaller time-step corresponds to $CFL_{\max} = 1$, based on the maximum instantaneous vertical velocity, v, and Δy at the flat plate trailing edge. Hence the larger time step corresponds to $CFL_{\max} = 10$. Moreover, a simulation with 2% blend of a second order upwind scheme and a 98% central differentiating scheme (CDS) and another simulation with a

5% blend of a second order upwind scheme and a 95% CDS in the full domain was made to evaluate the influence of upwind discretization. On the fine grid most simulations were made using CDS. However, one simulation was made using a second order upwind scheme in the RANS region on the flat plate upstream of the trailing edge and CDS in the LES region downstream of the flat plate trailing edge to follow the discretization approach used in the simulations of channel flow using embedded LES.

Table 5: Discretization schemes and time steps used in mixing layer simulations.

Grid	RANS	LES	Time step [s]
Coarse	CDS	CDS	5×10^{-5}
Coarse	CDS	CDS	5×10^{-4}
Coarse	2% upwind + 98% CDS	2% upwind + 98% CDS	5×10^{-5}
Coarse	5% upwind + 95% CDS	5% upwind + 95% CDS	5×10^{-5}
Fine	CDS	CDS	5×10^{-5}
Fine	2nd upwind	CDS	5×10^{-5}

The commutation terms in the k, ω and momentum equations are applied at the wall-normal embedded RANS-LES interface at $x = 0$. As a reference, simulations are used where no commutation terms are applied at the interface. This simulation is compared to simulations in which the commutation terms are applied in the k and ω equations and in the k, ω and momentum equations, respectively. The LES length scales used in the simulations are $\Delta = \Delta_{max}$ and $\Delta = \Delta_{\Omega}$, see Eqs. (9) and (10).

To evaluate the mixing layer growth, vorticity thickness and momentum thickness are used. These are defined as follows

$$\delta_{\omega} = \frac{U_a - U_b}{(\partial U/\partial y)_{y=0}} \tag{28}$$

$$\theta = \int_{-\infty}^{\infty} \frac{U - U_b}{U_a - U_b} \left(1 - \frac{U - U_b}{U_a - U_b}\right) dy \tag{29}$$

where, U_a and U_b are taken as the streamwise velocity at $y = -h$ and $y = h$.

The mixing layer growth for the coarse and fine grids are presented in Figs. 22-23. It can be seen that the effect of the applied commutation terms in combination with $\Delta = \Delta_{max}$ is more clear on the fine grid. It can also be seen that the effect of the commutation terms is stronger with $\Delta = \Delta_{max}$ than with $\Delta = \Delta_{\Omega}$.

When $\Delta = \Delta_{max}$ is used and no commutation terms are applied at the RANS-LES interface a poor mixing layer growth is predicted on the fine grid. The growth prediction is improved when adding the commutation terms in the k and ω equations. The best agreement to experimental data is given when commutation terms also are added in the momentum equations with $\Delta = \Delta_{max}$. The effect of using a second order upwind scheme in the RANS region instead of CDS on the fine grid is shown in Fig. 23. A delayed development of resolved turbulence in the trailing edge region is observed with the second order upwind scheme which contributes to a slightly slower growth of the vorticity and momentum thicknesses compared to the simulation using CDS in the whole domain.

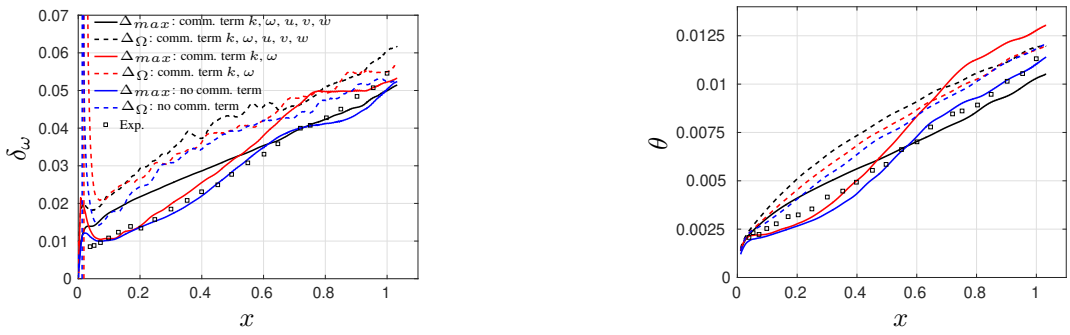

(a) Vorticity thickness

(b) Momentum thickness

Figure 22: Mixing layer. Growth of vorticity thickness and momentum thickness. Coarse grid.

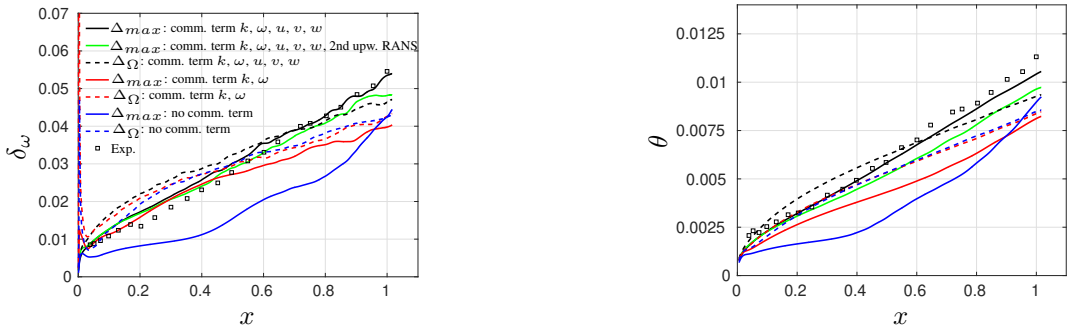

(a) Vorticity thickness (b) Momentum thickness

Figure 23: Mixing layer. Growth of vorticity thickness and momentum thickness. Fine grid.

When using Δ_Ω on the coarse grid, the mixing layer thickness is over predicted but with a growth rate that agrees reasonably well with the experiment. The vorticity thickness predicted with Δ_Ω is better aligned with the experimental data in the simulations made on the fine grid but the growth rate of the momentum thickness is too flat.

The poorly predicted momentum thickness on the coarse grid with Δ_{max} and the commutation terms applied in the k and ω equations is caused by a large scale flapping motion in the y direction of the mixing layer. The observed large scale flapping motion indicates that large unphysical turbulent structures are present in the mixing layer. This phenomenon is well known from the literature, see e.g. [9, 11], especially with the use of $\Delta = \Delta_{max}$ in the LES region. A tendency of a flapping motion, is also observed in the reference simulation with Δ_{max} on both the coarse and the fine grids. The tendency on the fine grid is weaker than on the coarse grid. When Δ_Ω is applied no such flapping motion is observed on either of the grids. The reason for the flapping motion is discussed below.

The time-averaged data presented is based on approximately four convective through flows (CTF) for the coarse grid, which seems too short to average out the strong flapping motion. For the simulation in which the commutation term is also included in the momentum equation, only two CTF were needed on the coarse grid for an accurate representation of the mean flow field. The statistical dataset used for the simulations on the fine grid is based on three CTF.

The large peaks observed in the vorticity thickness for Δ_Ω at the trailing edge with both grids is caused by strong velocity gradients (and velocity fluctuations). This peak is not observed for Δ_{max}, which is explained by the higher turbulent viscosity produced with this LES length scale in the trailing edge region, as can be seen in Fig. 24. The high turbulent viscosity reduces the strong velocity gradients and velocity fluctuations.

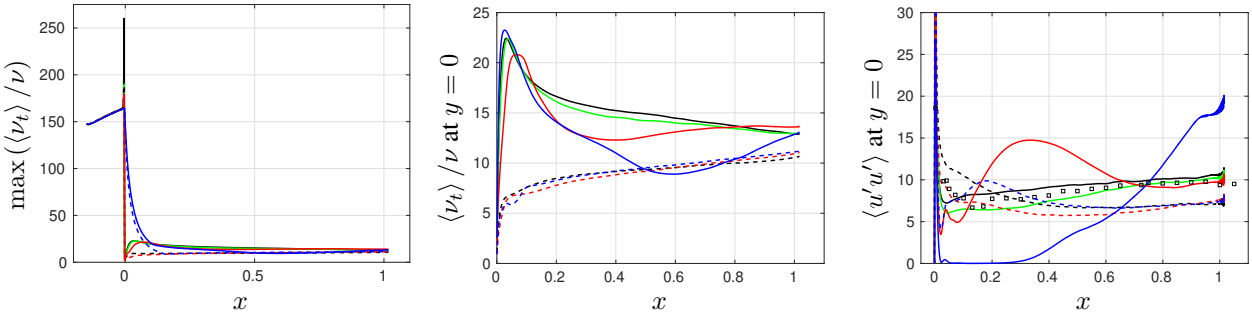

(a) $\max(\langle\nu_t\rangle/\nu)$. (b) $\langle\nu_t\rangle/\nu$ at $y = 0$. (c) $\langle u'u'\rangle$ at $y = 0$.

Figure 24: Mixing layer. Turbulent viscosity and resolved streamwise turbulent fluctuations along the x-direction. Fine grid. Colors as in Fig. 23.

The effect of discretization scheme and time step are evaluated with simulations on the coarse grid, which is shown in Fig. 25. It can be concluded that both LES length scales used are affected by the upwind discretization. Good results are given with 2% upwind blended with 98% CDS with Δ_Ω. However, this should be seen as a coincident and not a proper numerical setting for these types of flows. With 5% upwind and 95% CDS, Δ_Ω performs almost as poor as Δ_{max}. Hence, for an accurate prediction of the simulated mixing layer flow it can be concluded that the discretization scheme is critical; this is also concluded in e.g. Kok and van der Ven [9].

A weak influence of the larger time-step is observed for both LES length scales, as shown in Fig. 25. The weak influence also applies to the resolved turbulent stresses predicted (not shown).

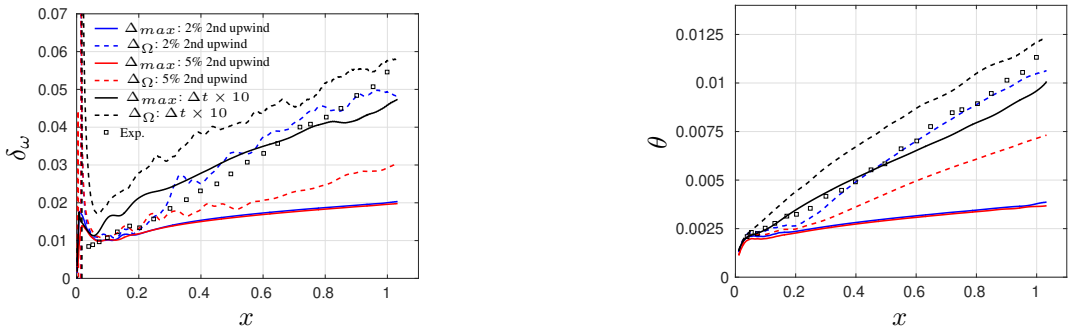

(a) Vorticity thickness (b) Momentum thickness

Figure 25: Mixing layer. Growth of vorticity thickness and momentum thickness. Coarse grid. Effect of upwind scheme and time step. Commutation terms in k and ω equations.

All simulations presented below are made on the fine grid. As in the simulations of channel flow and boundary layer flow, the commutation terms in the k and ω equations, presented in Fig. 26, rapidly reduce the turbulent viscosity across the embedded RANS-LES interface, as shown in Fig. 24 (a). The commutation and production terms in the k equation are of the same magnitude for this flow as well. When the commutation term is also added in the momentum equations, the magnitudes of the commutation and production terms in the k equation increase. It is also observed for this flow that the introduction of the commutation terms in the k and ω equations reduces the overall magnitude of the production term in the k equation.

The turbulent kinetic energy along x is presented in Fig. 26 (c) to show the effect of the commutation terms across the embedded RANS-LES interface and the effect on the flow far downstream of the trailing edge. As in Fig. 24 (c), which shows the maximum resolved streamwise fluctuations, the resolved turbulent kinetic energy is almost negligible from the trailing edge to $x = 0.4$ m for the case where $\Delta = \Delta_{max}$ and no commutation terms are added at the embedded RANS-LES interface. Downstream of this location the resolved turbulent kinetic energy grows rapidly for this simulation due to the observed unphysical large-scale fluctuations and takes the largest values of all simulations at $x = 1$ m. In the other simulations, especially in the simulations where the commutation term is added in the momentum equation, the level of the resolved turbulent kinetic energy grows continuously along x as expected. Moreover, the level of resolved turbulent energy is dominating over the modeled part in the LES region except for the case where $\Delta = \Delta_{max}$ and no commutation terms are used.

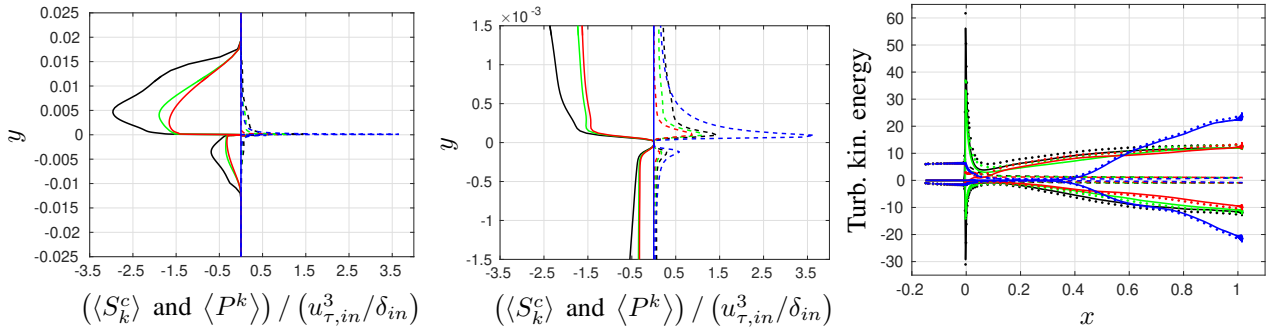

(a) Commutation and production terms. (b) Commutation and production terms, zoomed view. (c) Turbulent kinetic energy.

Figure 26: Mixing layer. Fine grid. Colors as in Fig. 23. (a) and (b) Commutation terms in the k equation at the embedded RANS-LES interface, $x = 0$, using $\Delta = \Delta_{max}$. Solid lines are commutation term and dashed lines are production term. (c) Resolved (solid), modeled (dashed) and total (dotted) kinetic energy at $y = -6 \times 10^{-3}$ m (lower boundary layer, plotted as negative values) and $y = 6 \times 10^{-3}$ m (upper boundary layer, plotted as positive values).

A much lower turbulent viscosity is observed in the trailing edge region in Fig. 24 (b) when $\Delta = \Delta_\Omega$ instead of $\Delta = \Delta_{\max}$. This explains the weaker effect of the commutation terms when Δ_Ω is applied. The low turbulent viscosity produced by Δ_Ω also contributes the large peaks in the resolved streamwise fluctuations observed at the trailing edge in Fig. 24 (c).

When the commutation term is added in the momentum equation as well, it works efficiently as a turbulence generator at the embedded RANS-LES interface. The initial two-dimensional turbulent structures, which are present shortly downstream of the trailing edge of the flat plate, seem to break up. Due to the break-up of the large scale turbulent structures, the establishment of the resolved turbulent stresses takes place quickly and sustain throughout the whole domain with $\Delta = \Delta_{max}$, as can be seen in Fig. 24 (c).

The commutation terms in the momentum equations increase the production of the modeled turbulent kinetic energy at the interface. The peak in the turbulent viscosity at the interface shown in Fig. 24 (a) is thus caused by the commutation terms in the momentum equations. For the same reason, there is a more rapid growth of the SGS turbulent viscosity shortly downstream of the trailing edge with the commutation terms applied in the momentum equations as compared to the simulation where the commutation terms are added only in the k and ω equations.

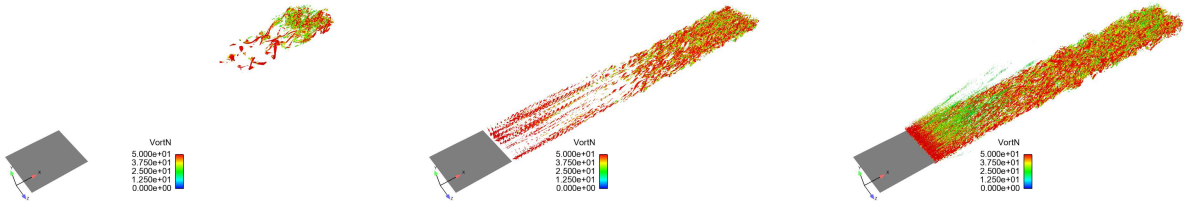

(a) No commutation terms. (b) Commutation terms in k and ω equations. (c) Commutation terms in k, ω, u, v and w equations.

Figure 27: Mixing layer. Effect of commutation terms at the RANS-LES interface located at the flat plate trailing edge. $\Delta = \Delta_{max}$. Resolved turbulent structures visualized using iso-surface of Q-criterion, $Q\left(L_{ref}/U_{low}\right)^2 = 100$, colored by the normalized vorticity magnitude, $\Omega\left(L_{ref}/U_{low}\right)$. Fine grid.

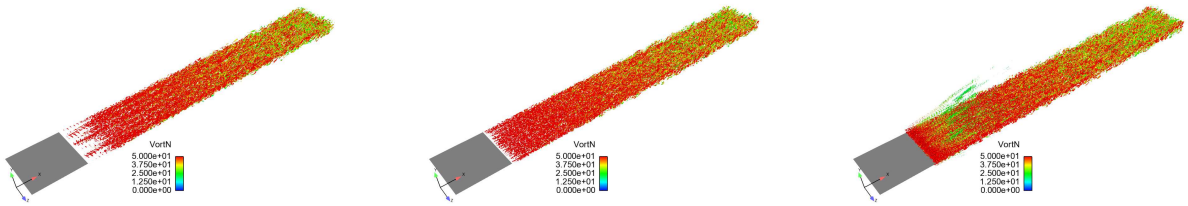

(a) No commutation terms. (b) Commutation terms in k and ω equations. (c) Commutation terms in k, ω, u, v and w equations.

Figure 28: Mixing layer. Effect of commutation terms at the RANS-LES interface located at the flat plate trailing edge. $\Delta = \Delta_{\Omega}$. Resolved turbulent structures visualized using iso-surface of Q-criterion, $Q\left(L_{ref}/U_{low}\right)^2 = 100$, colored by the normalized vorticity magnitude, $\Omega\left(L_{ref}/U_{low}\right)$. Fine grid.

The strong effect of the commutation terms on the resolved turbulent structures are illustrated using the Q-criterion in Figs. 27 and 28. The LES length scale $\Delta = \Delta_{max}$ gives a higher turbulent viscosity compared to $\Delta = \Delta_{\Omega}$ as seen in Fig. 24. An unphysical delay in the formation of resolved turbulence, the so-called grey area, is given without the generation of turbulent fluctuations from the commutation term in the momentum equation and the higher turbulent viscosity obtained with $\Delta = \Delta_{max}$. This delay and the large scale turbulent structures far downstream of the trailing edge, which are clearly illustrated in Fig. 27 (a)-(b), give the large-scale flapping motion referred to above. The absence of resolved turbulence with $\Delta = \Delta_{max}$ in the early stages of the free shear layer is also supported by the two-point correlations given in Fig. 29. With $\Delta = \Delta_{\Omega}$, smaller turbulent structures are resolved already near the trailing edge in contrast to $\Delta = \Delta_{max}$ as seen in Fig. 28, which explains why no large-scale flapping motions arises for this LES length scale. Small structures are observed outside of the shear layer in the trailing edge region in Fig. 27 (c) and 28 (c). These originates from numerical oscillations due to the strength of the commutation terms in the momentum equations.

The streamwise velocity field is presented in Fig. 30. The minor differences seen in the velocity profiles at $x = 1.5$ mm are expected since the boundary layers upstream of the embedded interface are simulated with RANS. At $x = 200$ and 500 mm, the simulation using Δ_{max} without commutation terms at the embedded RANS-LES interface differs from the velocity profiles predicted by the other simulations. At $x = 800$ mm, the simulations, in which the commutation terms are introduced in the momentum equations, predicts velocity profiles in best agreement with experimental data. However,

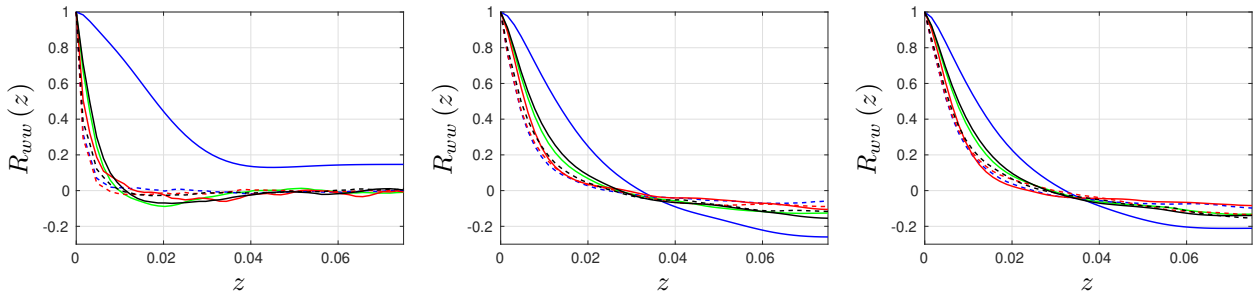

(a) $x = 200$ mm. (b) $x = 650$ mm. (c) $x = 800$ mm.

Figure 29: Mixing layer. Spanwise two-point correlations, $R_{ww}(z)$, at $y = 0$. Fine grid. Colors as in Fig. 23.

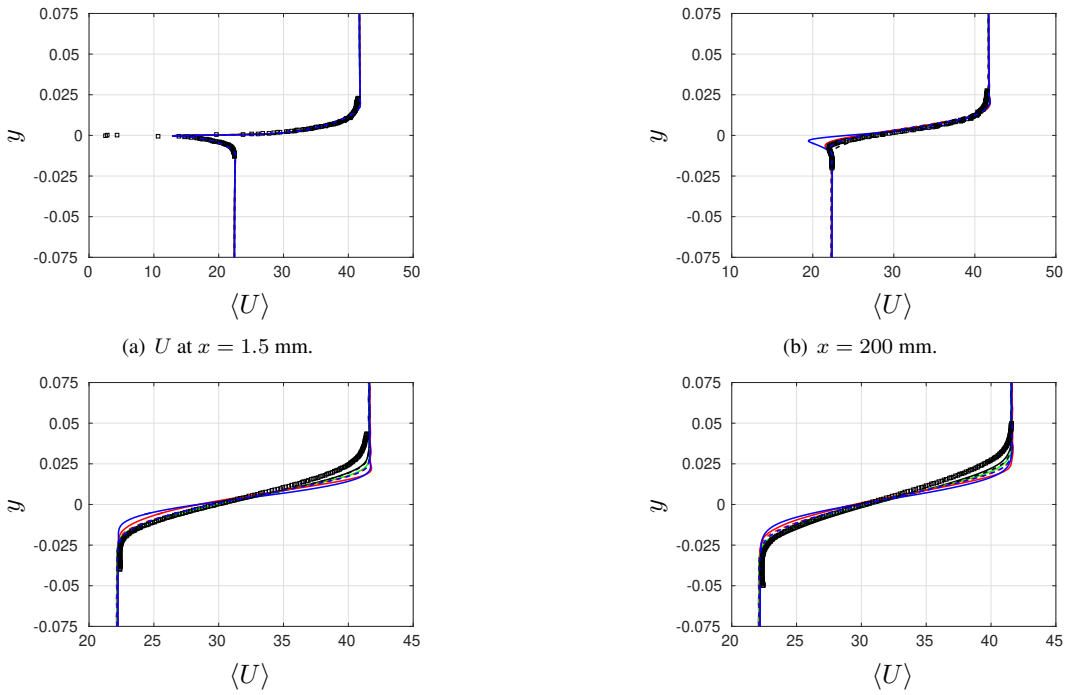

(a) U at $x = 1.5$ mm. (b) $x = 200$ mm.

(c) $x = 650$ mm. (d) $x = 800$ mm.

Figure 30: Mixing layer. Streamwise velocity, $\langle U \rangle$ m/s. Fine grid. Colors as in Fig. 23.

no large differences are observed between the simulations at this location.

With $\Delta = \Delta_{max}$ an improved prediction of the resolved turbulent stresses is given when the commutation terms are added in the k, ω and momentum equations. The resolved stresses presented are in very good agreement with experimental data, as seen in Fig. 31-34. With $\Delta = \Delta_\Omega$, the resolved turbulent stresses are slightly under-predicted in all simulations, except for $x \leq 200$ mm where the lower turbulent viscosity level makes the resolved normal stresses in the vertical and spanwise direction to develop rapidly and thus agree well with the experimental data. It is also observed that with $\Delta = \Delta_\Omega$ the influence of the commutation terms are weaker than with $\Delta = \Delta_{max}$.

The resolved streamwise normal stresses are strongly over-predicted at the center line at $x = 1.5$ mm in all simulations, especially when $\Delta = \Delta_\Omega$, as seen in Fig. 31 (a). The greater over-prediction with Δ_Ω as compared to Δ_{max} is caused by the lower turbulent viscosity predicted with this length scale at the trailing edge.

The effect of the commutation terms in the momentum equations is clearly observed in Fig. 31 (a). The commutation terms triggers resolved turbulence in a region as thick as the trailing edge boundary layer. The turbulent fluctuations produced is however over-predicted compared to the experimental data.

A great over-prediction of the resolved fluctuations in the vertical direction is observed for the reference simulation with $\Delta = \Delta_{max}$ at $x = 650$ and 800 mm, see Fig. 32, indicating a flapping motion as on the coarse grid. For this simulations also the resolved normal stresses in the vertical and the spanwise directions are almost negligible at $x = 200$

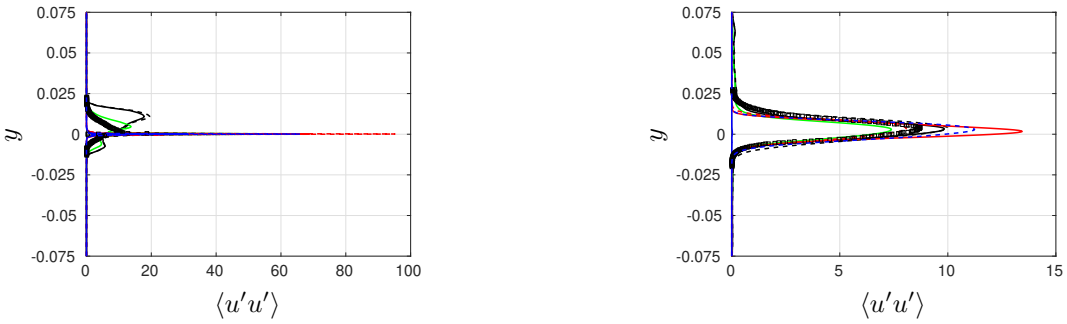

(a) $x = 1.5$ mm.

(b) $x = 200$ mm.

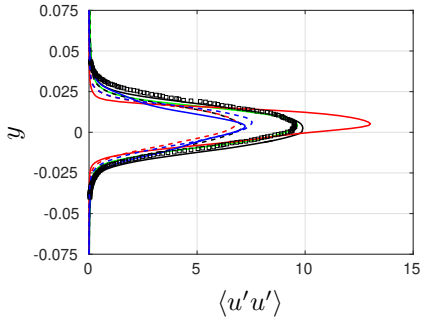

(c) $x = 650$ mm.

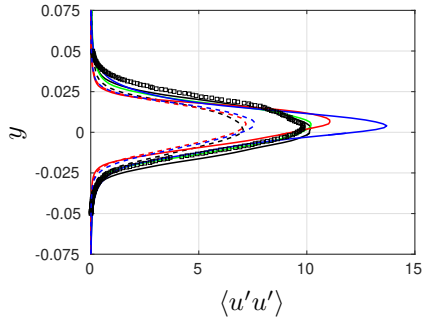

(d) $x = 800$ mm.

Figure 31: Mixing layer. Resolved streamwise velocity fluctuations. Fine grid. Colors as in Fig. 23.

mm, which shows the importance of adding the commutation terms at the RANS-LES interface to speed up the formation of the resolved turbulent stresses with $\Delta = \Delta_{max}$.

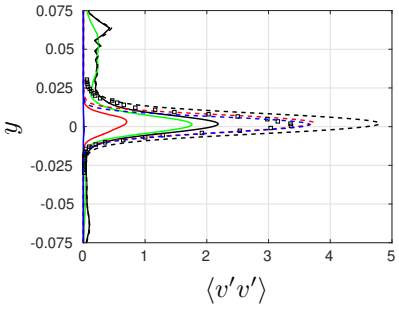

(a) $\langle v'v' \rangle$, $x = 200$ mm.

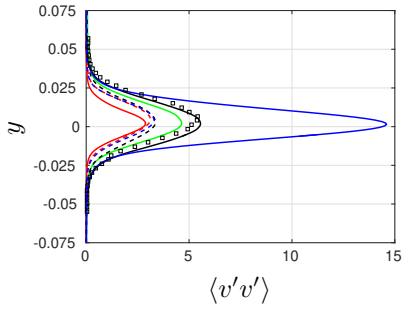

(b) $\langle v'v' \rangle$, $x = 650$ mm.

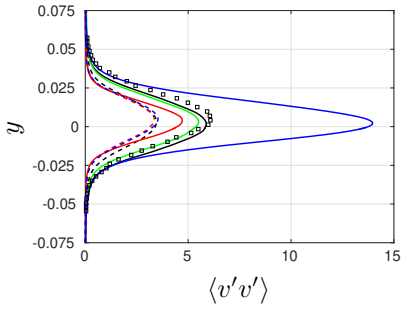

(c) $\langle v'v' \rangle$, $x = 800$ mm.

Figure 32: Mixing layer. Resolved velocity fluctuations, $\langle v'v' \rangle$. Fine grid. Colors as in Fig. 23.

The modeled shear stress is included in Fig. 34 (note that to enhance the readability it is plotted with opposite sign to the resolved stress). It can be seen that the modeled part, τ_{12}, is almost negligible as compared to the resolved part for the two most downstream locations. At $x = 200$ mm, $\Delta = \Delta_{max}$ gives a higher level of turbulent viscosity, hence also a higher level of the modeled shear stress compared to $\Delta = \Delta_\Omega$. The effect of the LES length scale on the modeled shear stress is more pronounced on the coarse grid where a higher level of modeled shear stress is obtained for Δ_{max}.

The power spectra density (PSD) of u' at $x = 200$ and 800 mm are given in Fig. 36 for simulations where commutation terms are used in k and ω as well as in the momentum equations on the fine grid. All threes simulations agree well with the experimental data, even thought the high frequencies are not resolved in the simulations. The PSD results for the given simulations also agree well with other simulations in the literature, see e.g. [9].

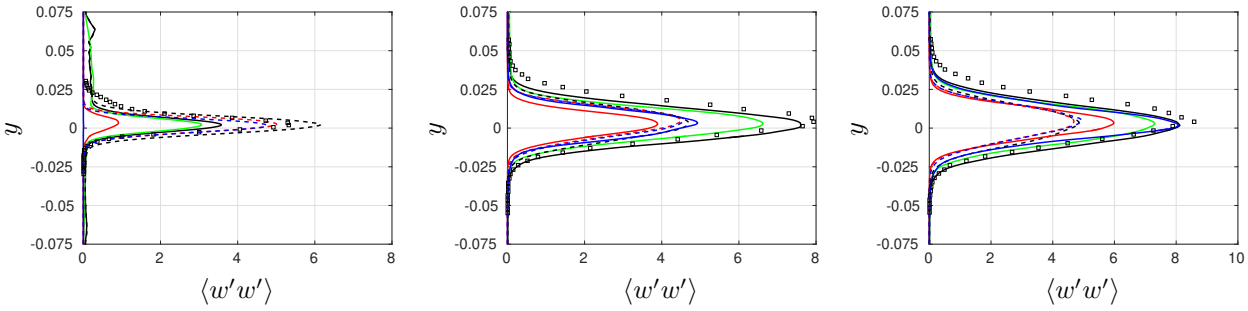

(a) $\langle w'w' \rangle$, $x = 200$ mm. (b) $\langle w'w' \rangle$, $x = 650$ mm. (c) $\langle w'w' \rangle$, $x = 800$ mm.

Figure 33: Mixing layer. Resolved velocity fluctuations, $\langle w'w' \rangle$. Fine grid. Colors as in Fig. 23.

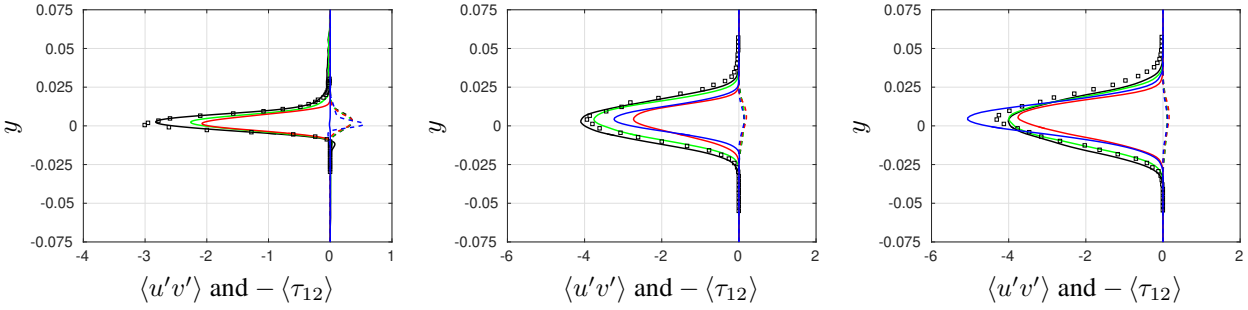

(a) $x = 200$ mm. (b) $x = 650$ mm. (c) $x = 800$ mm.

Figure 34: Mixing layer. Resolved ($\langle u'v' \rangle$, solid) and modeled ($\langle \tau_{12} \rangle$, dashed) turbulent shear stress using $\Delta = \Delta_{max}$. Fine grid. Colors as in Fig. 23.

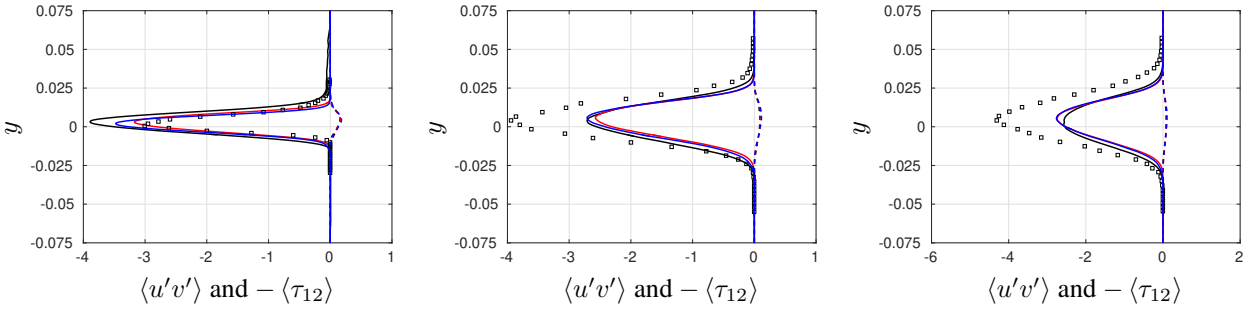

(a) $x = 200$ mm. (b) $x = 650$ mm. (c) $x = 800$ mm.

Figure 35: Mixing layer. Resolved ($\langle u'v' \rangle$, solid) and modeled ($\langle \tau_{12} \rangle$, dashed) turbulent shear stress using $\Delta = \Delta_{\Omega}$. Fine grid. Colors as in Fig. 23.

4 Conclusions

A low-Reynolds-number $k - \omega$ based hybrid RANS-LES turbulence model was used to evaluate the use of commutation terms at the RANS-LES interfaces, with the aim to mitigate the grey area. The proposed methodology is evaluated in embedded LES simulations of channel flow, boundary layer flow and mixing layer flow. The commutation terms have been applied to the convection terms in the k, ω and momentum equations at wall-normal and wall-parallel RANS-LES interfaces.

The methodology involves no empirical constants or functions. Moreover, the methodology is not fine tuned for the $k - \omega$ based hybrid RANS-LES turbulence model used or for the simulated flow cases. Hence, the proposed grey-area mitigation method is general and can be applied to any transport equation based hybrid RANS-LES turbulence model.

The effect of the commutation terms in the k and ω equations is to reduce the turbulent viscosity on the LES side of the interface and increase the turbulent viscosity on the RANS side of the RANS-LES interface. The commutation

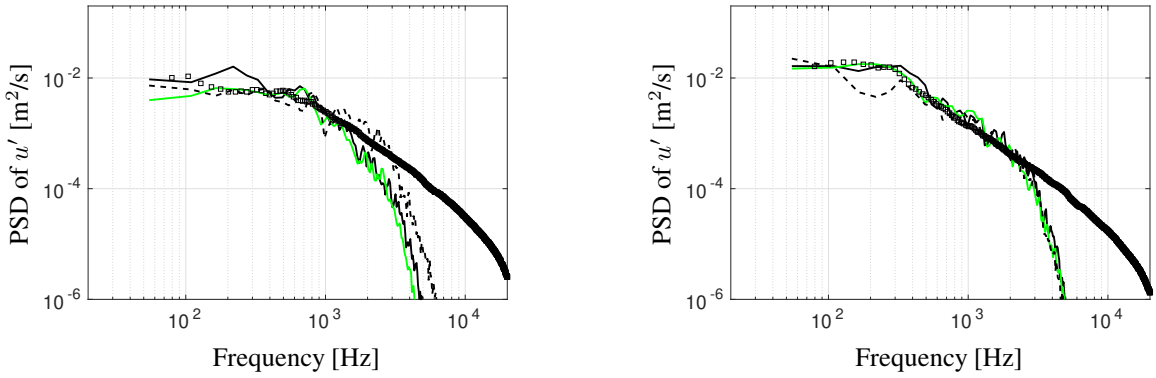

(a) $x = 200$ mm.

(b) $x = 800$ mm.

Figure 36: Mixing layer. PSD of u' at $(y, z) = (0, z_{\max}/2)$. Fine grid. Colors as in Fig. 23. Markers are experimental data.

term in the momentum equations act as a generator of resolved turbulence in order to compensate for the reduction of the modeled turbulent kinetic energy across the RANS-to-LES interface.

At the wall-normal embedded interface in the channel flow simulations and at the inflow boundary in the boundary layer simulations, the commutation terms in the k and ω equations are applied along with synthetic turbulent fluctuations. At the embedded interface in the mixing layer flow, commutation terms in the k, ω and momentum equations are applied without any synthetic turbulent fluctuations.

In all three flow cases presented, the commutation terms in the k and ω equations applied to the wall-normal interfaces rapidly reduce the turbulent viscosity. It is concluded also that the magnitude of the commutation term at these interfaces in the k equation is much larger than the magnitude of the production term as well as the diffusion and dissipation terms for $y^+ > 20$. At the wall-parallel RANS-LES interfaces (channel flow and boundary layer flow), the magnitudes of the commutation, production, diffusion and dissipation terms in the k equation are of the same magnitude.

In the simulations of the boundary layer flow, the use of the commutation terms in the k and ω equations at the inlet gives a shorter recovery length than when the commutation terms are not applied. The advantage of the commutation terms applied at the wall-normal embedded RANS-LES interface in the channel flow simulations is less clear. A fully developed flow is not reached in any of the channel flow simulations. However, no large differences are observed for the simulated channel lengths, with or without applying the commutation term at the wall-normal interface.

The effect of the different wall-normal interface treatments in the channel flow simulations is of the same magnitude as the effect of the wall-parallel interface treatments. In the boundary layer simulations, the flow reaches a fully developed state and the different wall-parallel interface treatments give clear differences in the predicted skin friction distributions. The shortest recovery length with a reasonably well predicted skin friction level is produced when no commutation terms are applied at the wall-parallel interface. However, all the simulations that are presented predict a skin friction distribution within 5% compared to the Coles-Fernholz correlation, which is used as a reference.

With the use of commutation terms in the k and ω equations on both sides of the wall-parallel RANS-LES interface, an amplified log-layer mismatch is given in the channel flow simulations and in the boundary layer simulations. A minor reduction of the log-layer mismatch is given if the commutation terms in the k, ω and momentum equations are applied on the LES side of the wall-parallel interface for these flows. Although the effect of the commutation terms at the wall-parallel interface is weak with respect to log-layer mismatch, a small log-layer mismatch is given already with the LES length scale used in these simulations also without any commutation terms. Moreover, it is concluded that the location of the wall-parallel interface affects the behavior of the commutation terms. With a wall-parallel RANS-LES interface closer to the wall, the commutations terms get stronger and hence better stimulates a turbulence-resolving flow than if the wall-parallel interface is located farther out from the wall.

With the use of the commutation terms in the k, ω and momentum equations at the embedded interface in the mixing layer simulations, it has been proven that there is a capability to quickly establish accurate resolved stresses. It can be concluded that the commutation terms in the k and ω equations reduce the turbulent viscosity at the trailing edge of the flat plate. However, this is not sufficient to achieve a rapid start-up of the resolved turbulence immediately downstream of the flat plate trailing edge. The turbulent fluctuations generated with the commutation terms in the momentum equations are needed in order to reduce the grey area with $\Delta = \Delta_{max}$. With $\Delta = \Delta_{max}$ and commutation terms in the k, ω and momentum equations, very good agreement with experimental data is obtained on the fine grid. The effect of the

commutation terms is much weaker with $\Delta = \Delta_\Omega$ since this length scale produces lower levels of turbulent viscosity. Moreover, it is concluded that the choice of discretization scheme is essential for an accurate prediction of the simulated mixing layer. A pure central scheme is needed to prevent damping the developing natural instabilities in the mixing layer simulations. With a blend of 5% second order upwind scheme with and a 95% central scheme, almost no resolved turbulent stresses were developed with either of LES length scales evaluated, and the growth rate of the mixing layer is much delayed.

Acknowledgement

This work has been funded by the Swedish Governmental Agency for Innovation Systems (VINNOVA), the Swedish Defence Materiel Administration (FMV) and the Swedish Armed Forces within the National Aviation Research Programme (NFFP, Contract No. 2013-01209 and 2017-04887) and Saab Aeronautics. The simulations were performed on resources provided by the Swedish National Infrastructure for Computing (SNIC) at the National Supercomputer Centre (NSC).

References

[1] P. R. Spalart and V. Venkatakrishnan. On the role and challenges of CFD in the aerospace industry. *The Aeronautical Journal*, 120(1223):209–232, 2016.

[2] P. Spalart, W-H. Jou, M. Strelets, and S.R. Allmaras. Comments on the feasability of les for wings, and on a hybrid rans/les approach. In *Advances in DNS/LES*, pages 137–147, Ruston, Lousiana, 1997.

[3] P.R. Spalart, S. Deck, M.L. Shur, K.D. Squires, M. Kh. Strelets, and A. Travin. A new version of detached-eddy simulation, resistant to ambiguous grid densities. *Theory of Computational Fluid Dynamics*, 20:181–195, 2006.

[4] M.L. Shur, P.R. Spalart, M.Kh. Strelets, and A.K. Travin. A hybrid RANS-LES approach with delayed-DES and wall-modelled LES capabilities. *International Journal of Heat and Fluid Flow*, 29:1638–1649, 2008.

[5] L. Davidson and S-H. Peng. Hybrid LES-RANS modelling: a one-equation SGS model combined with a $k-\omega$ model for predicting recirculating flows. *International Journal for Numerical Methods in Fluids*, 43:1003–1018, 2003.

[6] S. Deck. Recent improvments in the zonal detached eddy simualtion (ZDES) formulation. *Theoretical and Computational Fluid Dynamics*, 2011.

[7] S. Arvidson, L. Davidson, and S-H. Peng. Hybrid Reynolds-Averaged Navier-Stokes/Large-Eddy Simulation Modeling Based on a Low-Reynolds-Number $k-\omega$ Model. *AIAA Journal*, 54:4032–4037, 2016.

[8] C. Mockett, W. Haase, and F. Thiele. Go4hybrid: A European Initiative for Improved Hybrid RANS-LES Modelling. In S. Girimaji, W. Haase, S-H. Peng, and D. Schwamborn, editors, *Progress in Hybrid RANS-LES Modelling*, volume 130 of *NNFM*, pages 299–303, Cham, 2015. Springer International Publishing.

[9] J. Kok and H. van der Ven. Capturing free shear layers in hybrid rans-les simulations of separated flow. Technical Report NLR-TP-2012-333, National Aerospace Laboratory NLR, 2012.

[10] N. Chauvet, S. Deck, and L. Jaquin. Zonal Detached Eddy Simualtion of a Controlled Propulsive Jet. *AIAA Journal*, 45:2458–2473, 2007.

[11] C. Mockett, M. Fuchs, A. Garbaruk, M. Shur, P. Spalart, M. Strelets, F. Thiele, and A. Travin. Two Non-zonal Approaches to Accelerate RANS to LES Transition of Free Shear Layers in DES. In S. Girimaji, W. Haase, S-H. Peng, and D. Schwamborn, editors, *Progress in Hybrid RANS-LES Modelling*, volume 130 of *NNFM*, pages 187–201, Cham, 2015. Springer International Publishing.

[12] Mikhail L. Shur, Philippe R. Spalart, Mikhail Kh. Strelets, and Andrey K. Travin. An enhanced version of des with rapid transition from rans to les in separated flows. *Flow, Turbulence and Combustion*, 95(4):709–737, 2015.

[13] S. Arvidson, L. Davidson, and S.-H. Peng. Hybrid RANS-LES Modeling Using a Low-Reynolds-Number $k-\omega$ Based Model. AIAA paper 2014-0225, National Harbour, Maryland, 2014.

[14] F. Hamba. Analysis of filtered Navier-Stokes equation for hybrid RANS/LES simulation. *Physics of Fluids A*, 23, 2011.

[15] S. Girimaji and S. Wallin. Closure modeling in bridging regions of variable-resolution (VR) turbulence computations. *Journal of Turbulence*, 14(1):72–98, 2013.

[16] L. Davidson. Zonal PANS: evaluation of different treatments of the RANS-LES interface. *Journal of Turbulence*, 17(3):274–307, 2016.

[17] L. Davidson. Two-equation hybrid RANS-LES models: a novel way to treat k and ω at inlets and at embedded interfaces. *Journal of Turbulence*, 18(4):291–315, 2017.

[18] S-H. Peng, L. Davidson, and S. Holmberg. A Modified Low-Reynolds-Number $k-\omega$ Model for Recirculating Flows. *Journal of Fluids Engineering*, 119:867–875, 1997.

[19] L. Davidson. Two-equation hybrid RANS-LES Models: A novel way to treat k and ω at the inlet. In Hanjalic K. et al., editor, *Turbulence Heat and Mass Transfer, THMT-15*. Begell House Inc., New York, 2015.

[20] L. Davidson. The PANS k-ϵ model in a zonal hybrid RANS-LES formulation. *International Journal of Heat and Fluid Flow*, 46:112–126, 2014.

[21] L. Davidson. Using isotropic synthetic fluctuations as inlet boundary conditions for unsteady simulations. *Adv Appl Fluid Mech.*, 1(1):1–35, 2007.

[22] L. Davidson and S-H. Peng. Embedded Large-Eddy Simulation Using the Partially Averaged Navier-Stokes Model. *AIAA Journal*, 51:1066–1079, 2013.

[23] S. Wallin and A.V. Johansson. An explicit algebraic reynolds stress model for incompressible and compressible turbulent flows. *Journal of Fluid Mechanics*, 403:89–132, 2000.

[24] S. Arvidson, L. Davidson, and S-H. Peng. Grey-area mitigation using commutation terms at the interfaces in hybrid rans-les modeling. In Y. Hoarau, S-H. Peng, D. Schwamborn, and A. Revell, editors, *Progress in Hybrid RANS-LES Modelling*, volume 137 of *NNFM*, pages 113–124. Springer, 2018.

[25] P. Schlatter and R. Örlü. Assessment of direct numerical simulation data of turbulent boundary layers. *Journal of Fluid Mechanics*, 659:116–126, 2010.

[26] D.B. DeGraaff and J.K. Eaton. Reynolds number scaling of the flat-plate turbulent boundary layer. *Journal of Fluid Mechanics*, 422:319–346, 2000.

[27] J. Delville. *La décomposition orthogonale aux valeurs propres et l'analyse de l'organisation tridimensionnelle des écoulements turbulents ci saillés libres*. PhD thesis, Université de Poitiers, 1995.

[28] J. Matsfelt. Actuator turbine models and trailing edge flow: implementation in an in-house code. Master thesis 2015:76, Applied Mechanics, Chalmers University of Technology, 2015.

[29] S. Deck. Recent improvments in the zonal detached eddy simualtion (ZDES) formulation. *Theoretical and Computational Fluid Dynamics*, 2012.